US 20140364735A1

(19) **United States**

(12) **Patent Application Publication**

(10) **Pub. No.: US 2014/0364735 A1**

(43) **Pub. Date: Dec. 11, 2014**

Huang et al.

(54) **ULTRASOUND WAVEFORM TOMOGRAPHY WITH TV REGULARIZATION**

(71) Applicant: **LOS ALAMOS NATIONAL SECURITY, LLC**, Los Alamos, NM (US)

(72) Inventors: **Lianjie Huang**, Los Alamos, NM (US); **Youzuo Lin**, Los Alamos, NM (US)

(73) Assignee: **LOS ALAMOS NATIONAL SECURITY, LLC**, Los Alamos, NM (US)

(21) Appl. No.: **14/339,728**

(22) Filed: **Jul. 24, 2014**

Related U.S. Application Data

(63) Continuation of application No. PCT/US2013/024545, filed on Feb. 3, 2013.

(60) Provisional application No. 61/594,865, filed on Feb. 3, 2012.

Publication Classification

(51) **Int. Cl.**

A61B 8/08	(2006.01)
G06T 5/00	(2006.01)
A61B 8/15	(2006.01)

(52) **U.S. Cl.**

CPC ***A61B 8/0825*** (2013.01); ***A61B 8/15*** (2013.01); ***G06T 5/001*** (2013.01)

USPC **600/447**

(57) **ABSTRACT**

Synthetic-aperture ultrasound tomography systems and methods using scanning arrays and algorithms configured to simultaneously acquire ultrasound transmission and reflection data, and process the data for improved ultrasound tomography imaging, wherein the tomography imaging comprises total-variation regularization, or a modified total variation regularization.

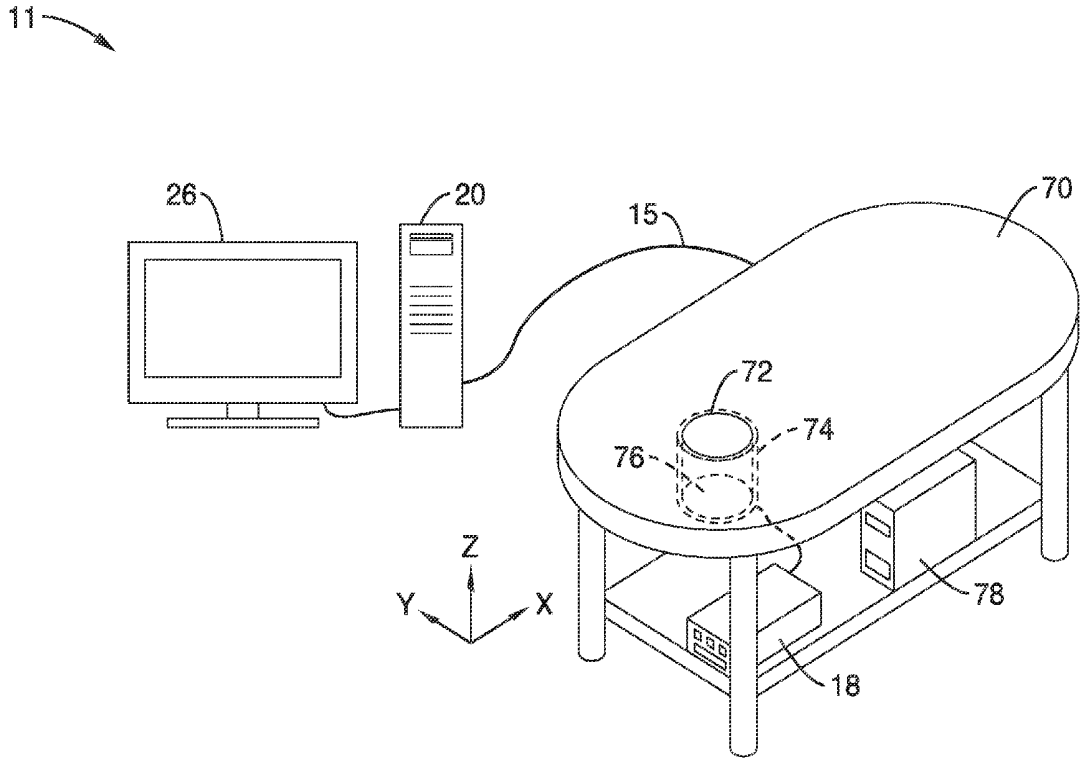

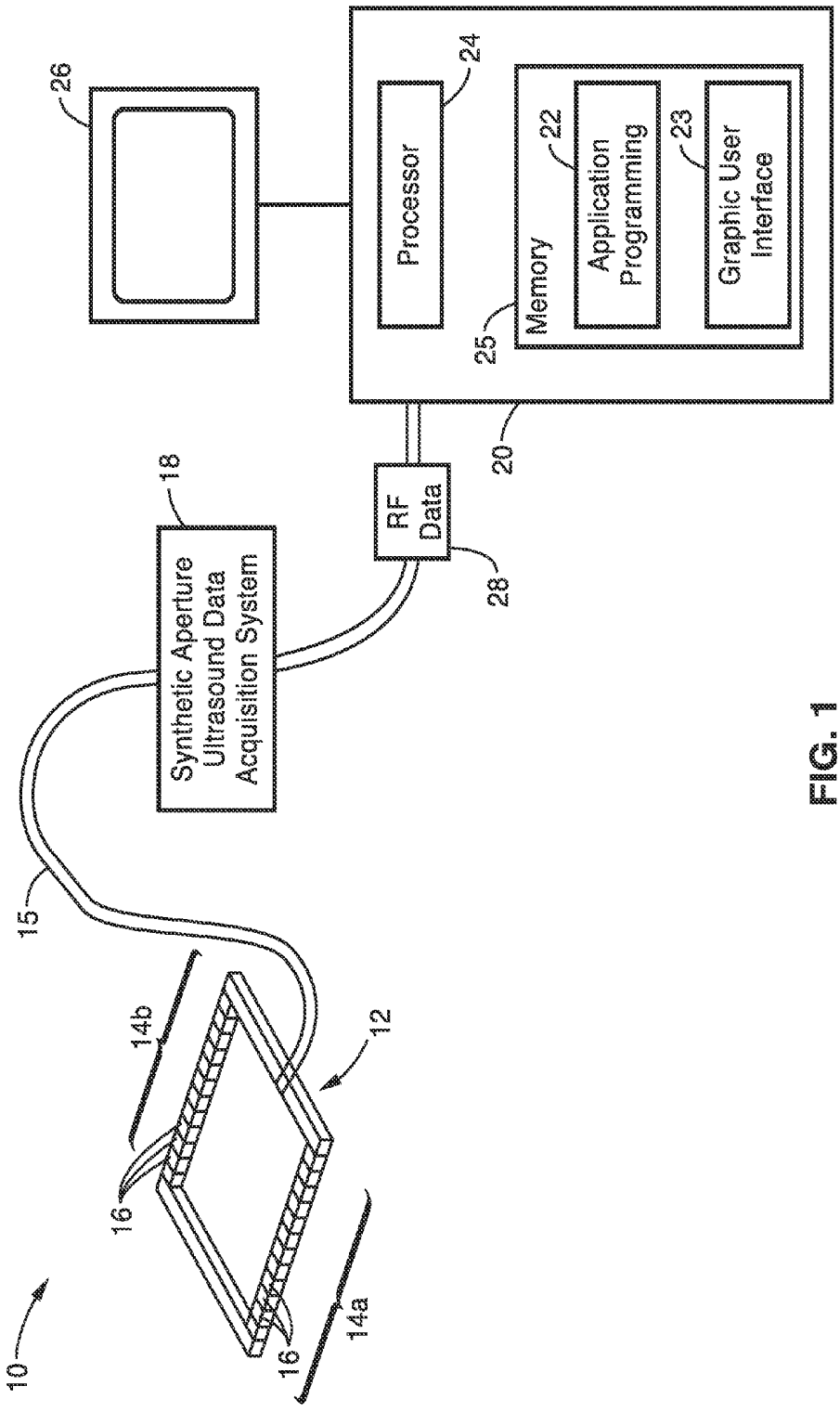
26
Processor
24
Memory
22
Application Programming
23
Graphic User Interface
25
20
RF Data
28
18
Synthetic Aperture Ultrasound Data Acquisition System
15
14b
12
16
16
14a
10

FIG. 1

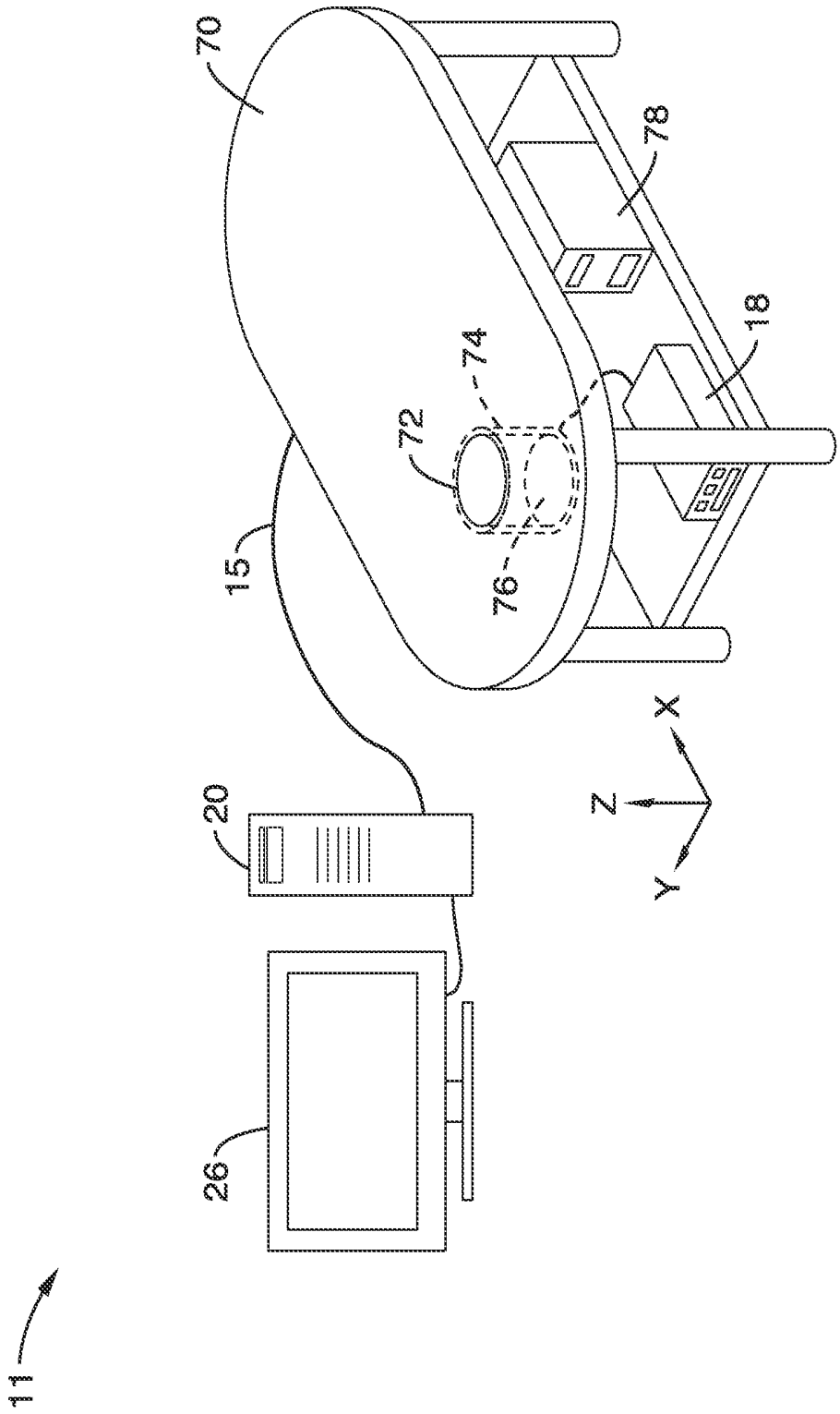

FIG. 2

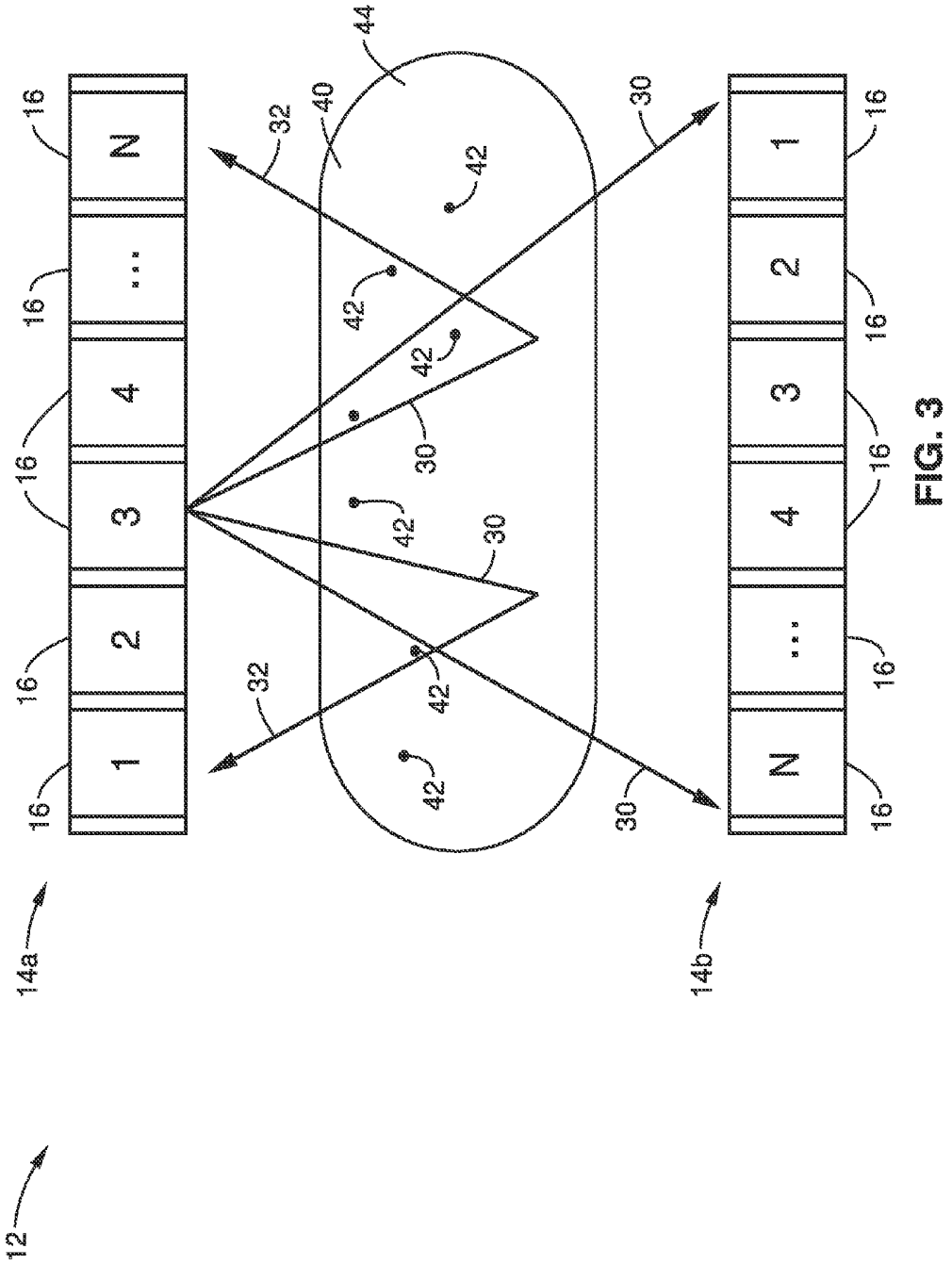

FIG. 3

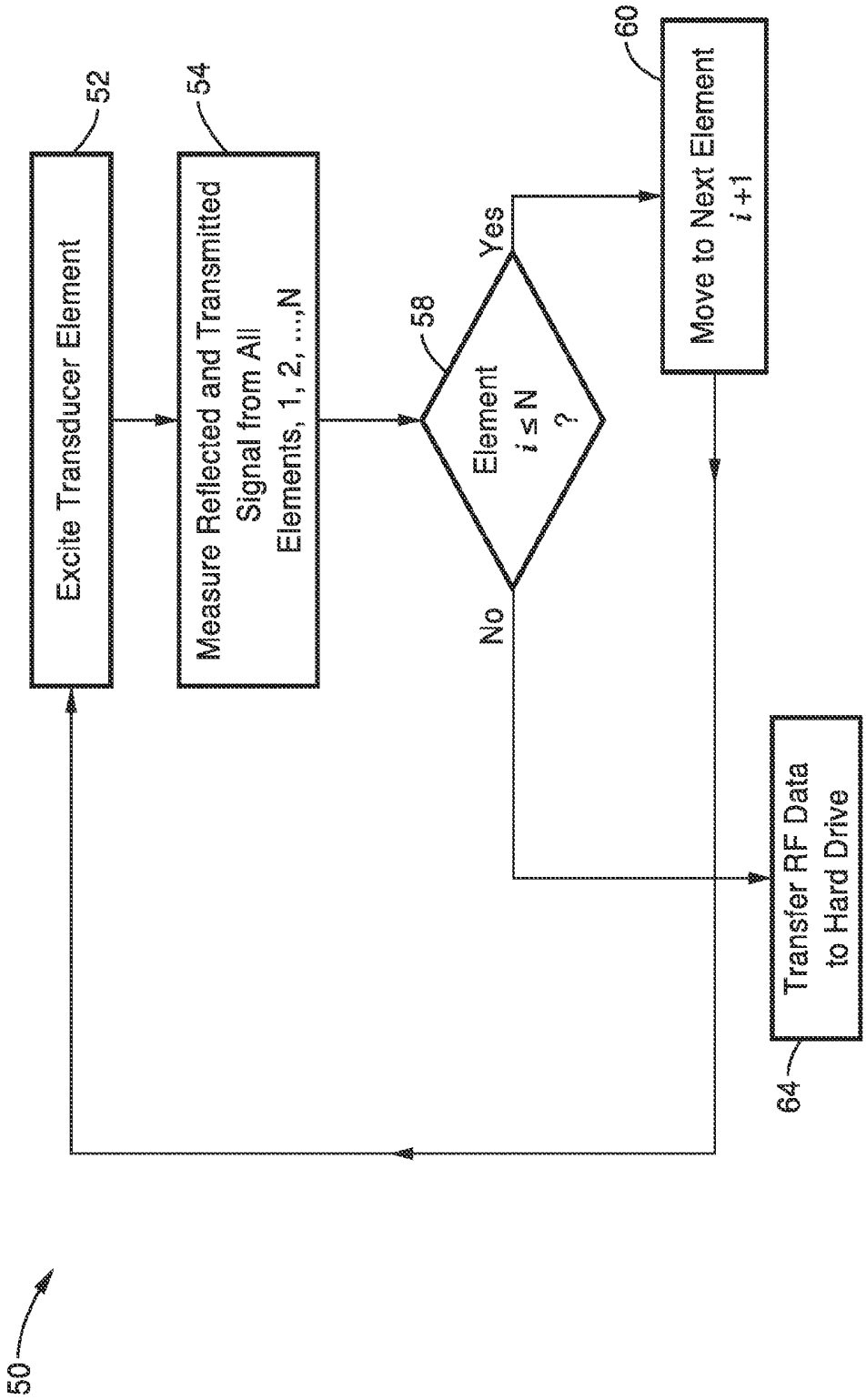
50
52
Excite Transducer Element
54
Measure Reflected and Transmitted Signal from All Elements, 1, 2, ...,N
58
Element $i \leq N$?
Yes
No
60
Move to Next Element $i+1$
64
Transfer RF Data to Hard Drive

FIG. 4

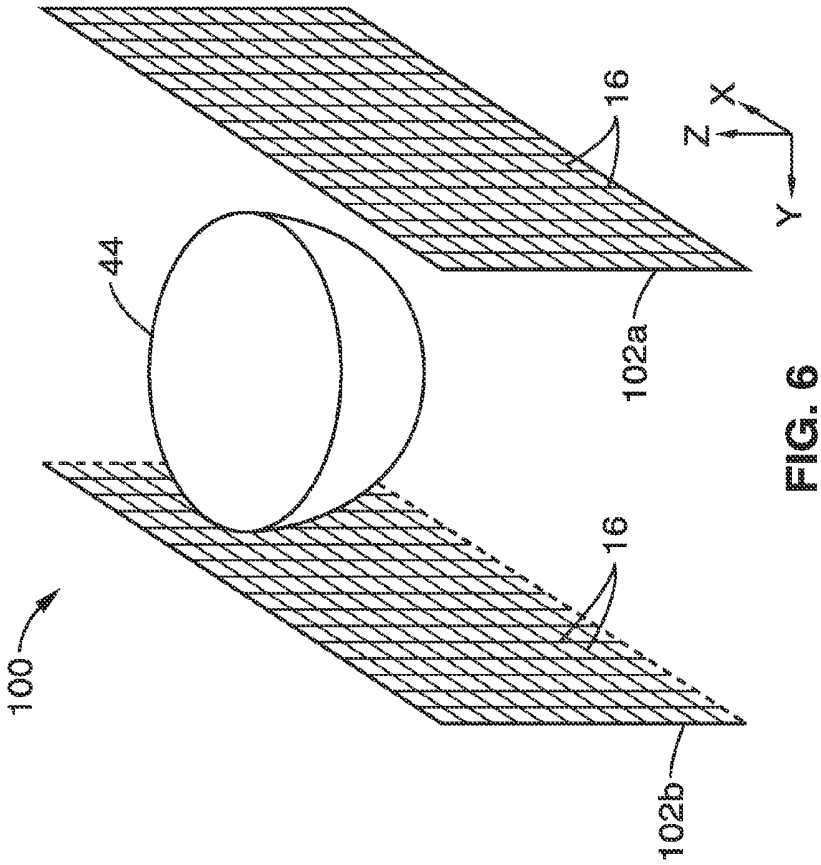

FIG. 6

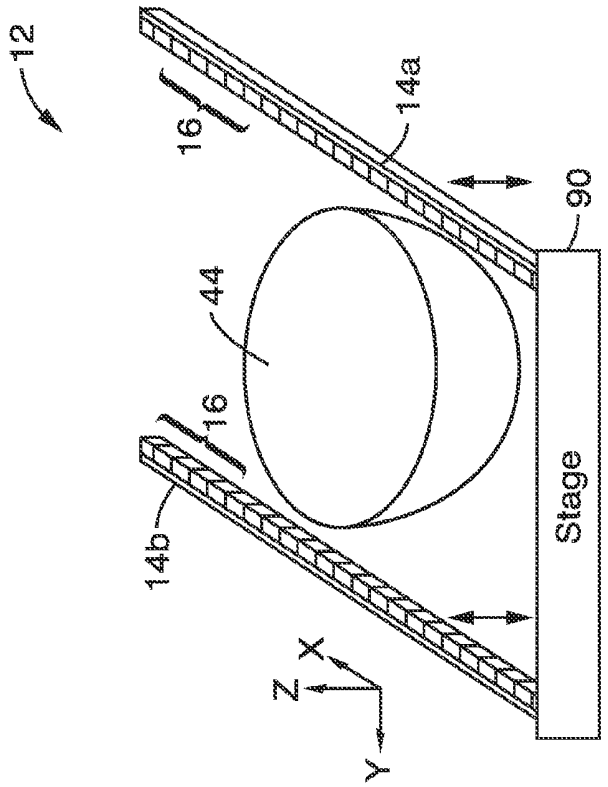

FIG. 5

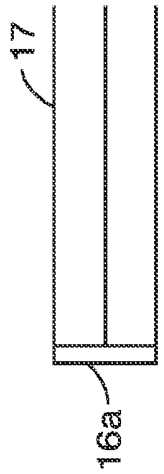

FIG. 8

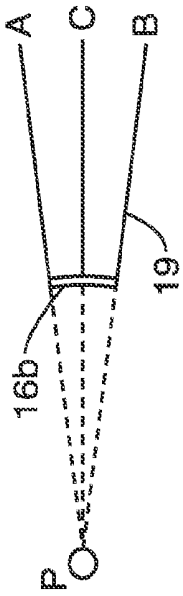

FIG. 9

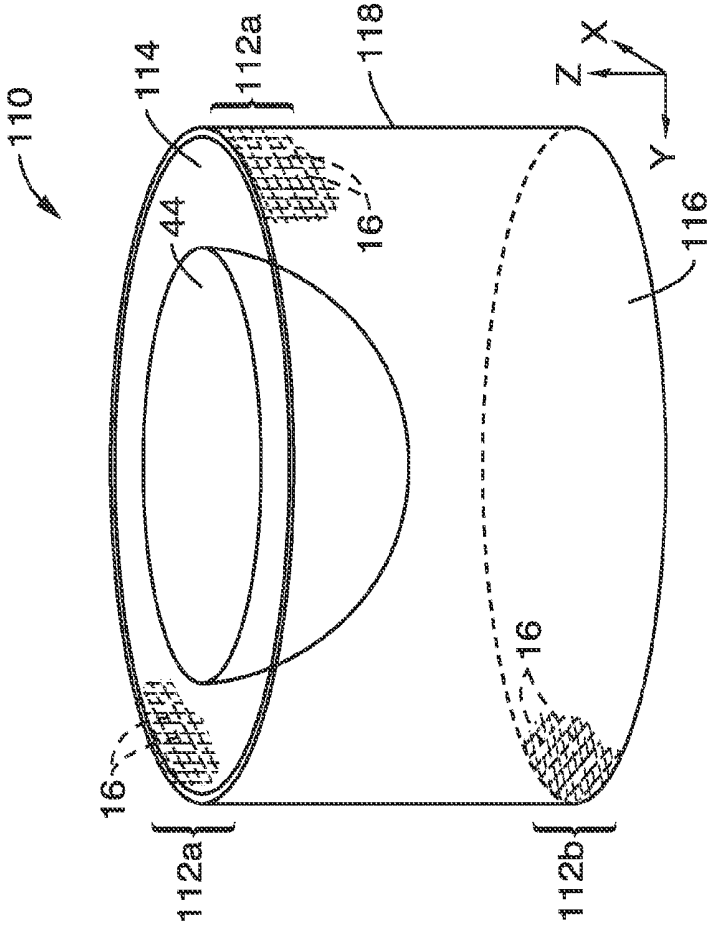

FIG. 7

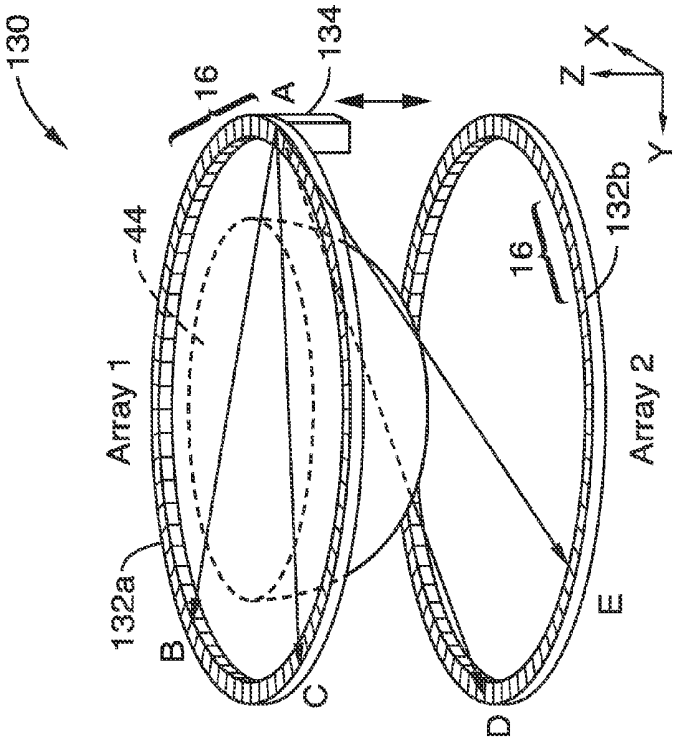
130
16
A
134
Z
X
Y
44
132b
16
Array 1
Array 2
132a
B
C
D
E

FIG. 11

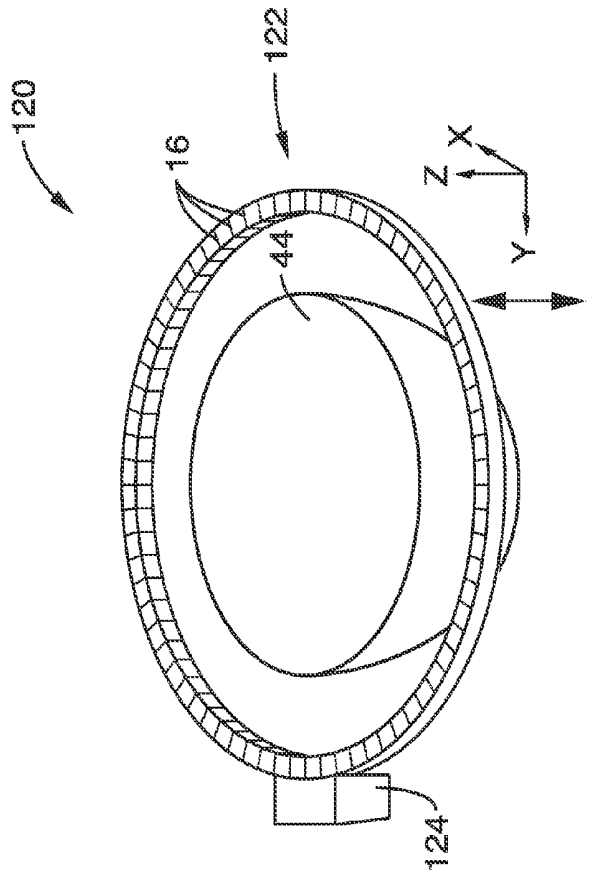
120
122
16
Z
X
Y
44
124

FIG. 10

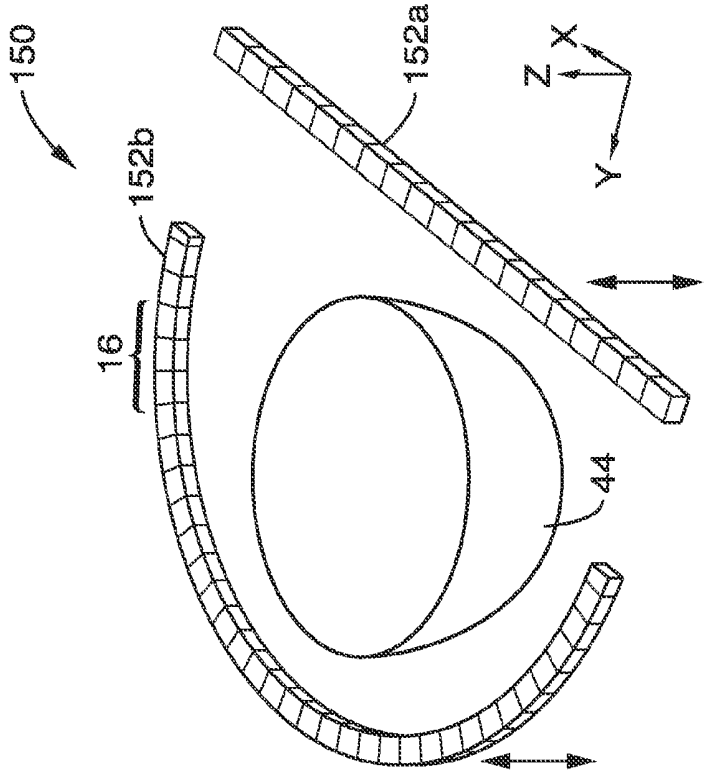

FIG. 13

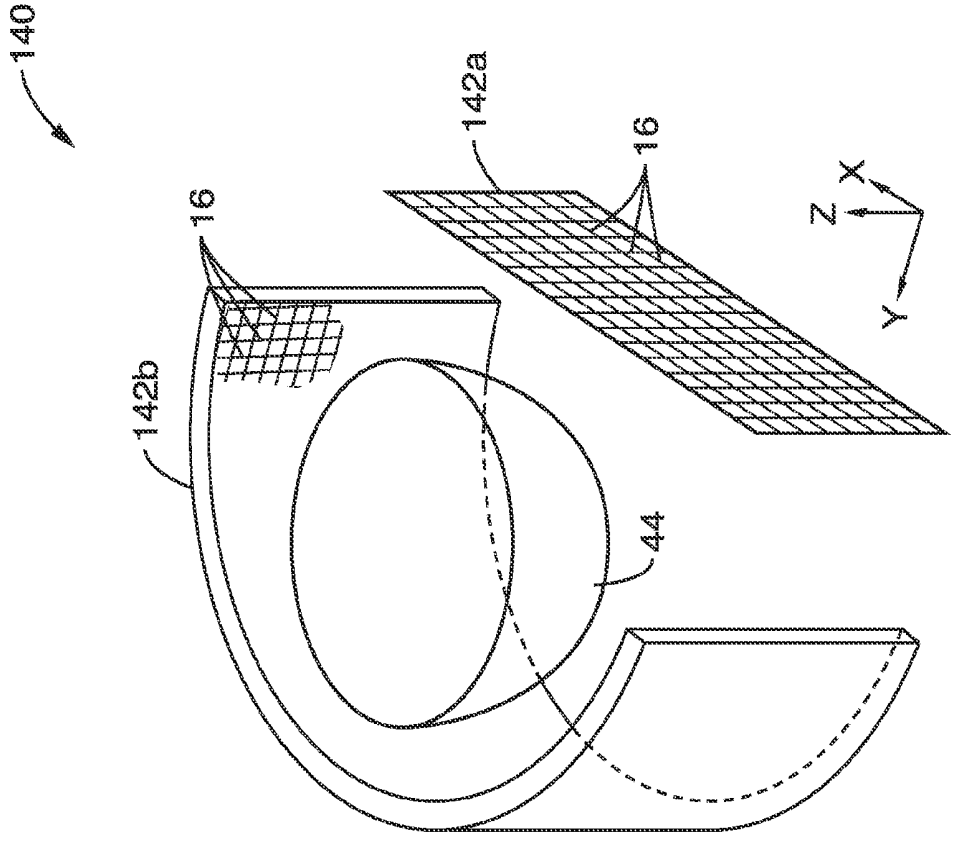

FIG. 12

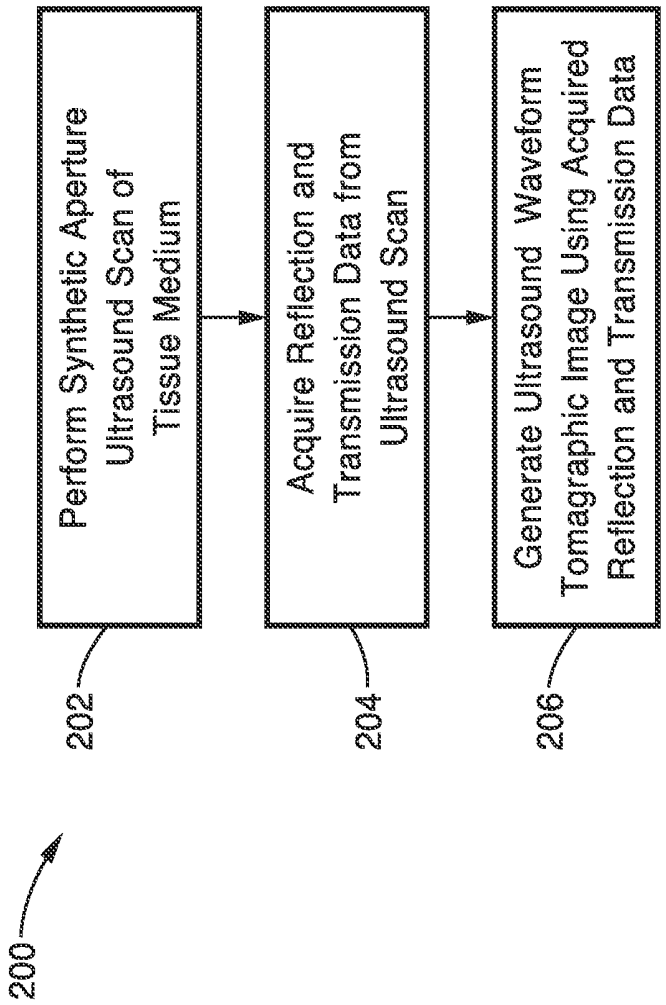
Perform Synthetic Aperture Ultrasound Scan of Tissue Medium
Acquire Reflection and Transmission Data from Ultrasound Scan
Generate Ultrasound Waveform Tomagraphic Image Using Acquired Reflection and Transmission Data
202
204
206
200

FIG. 14

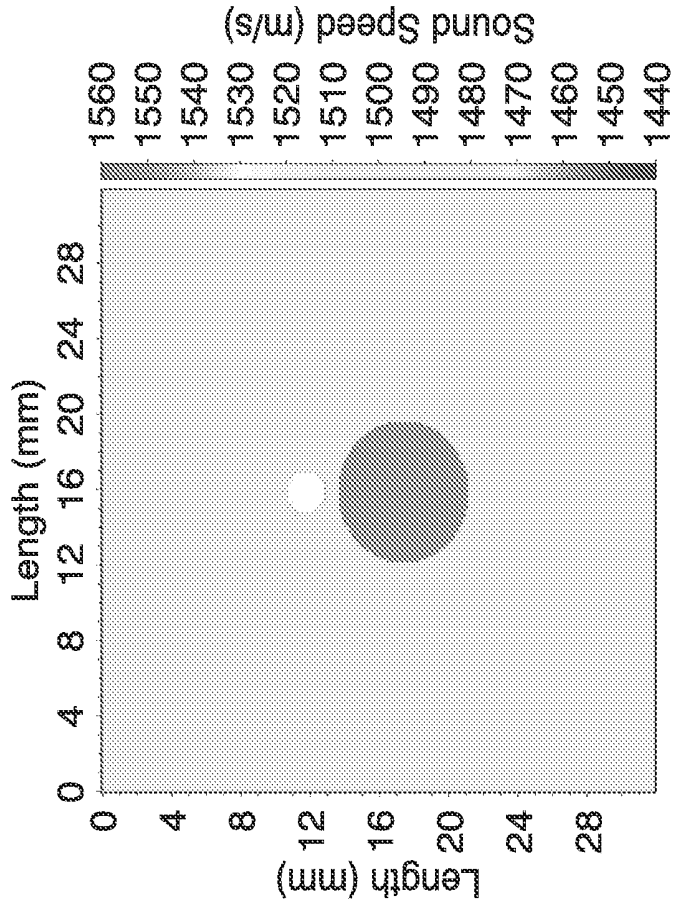
Sound Speed (m/s)
1560
1550
1540
1530
1520
1510
1500
1490
1480
1470
1460
1450
1440
Length (mm)
0
4
8
12
16
20
24
28
Length (mm)
0
4
8
12
16
20
24
28

FIG. 15

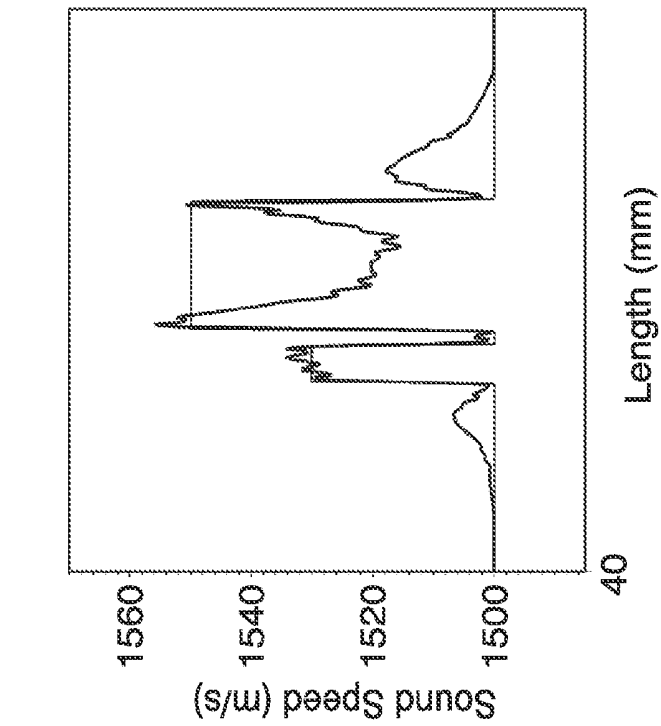

FIG. 16B

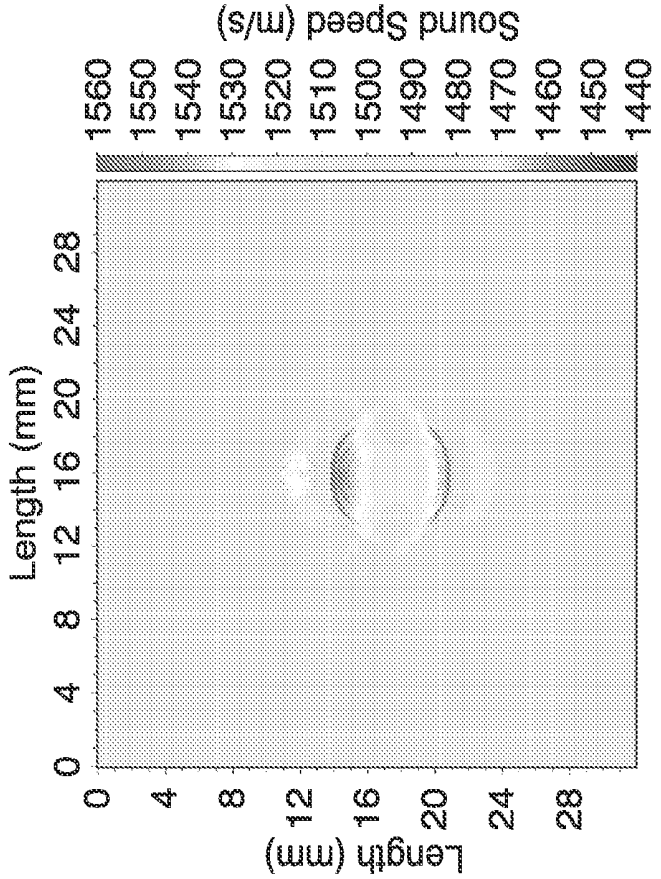

FIG. 16A

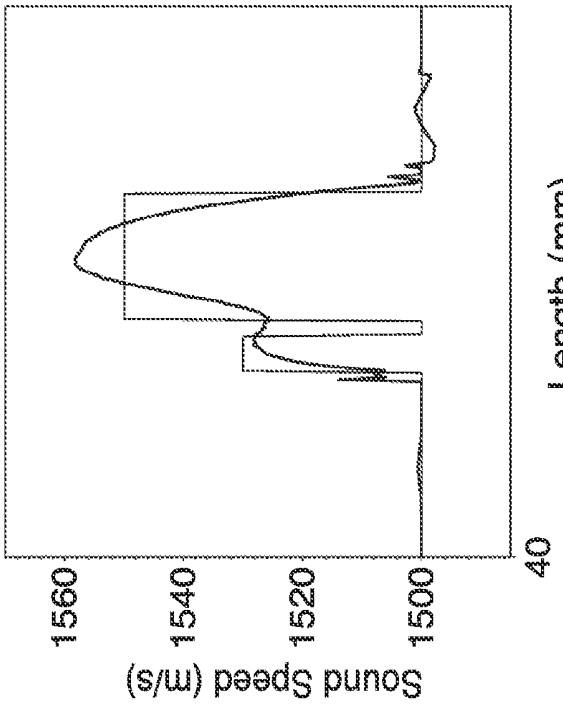

FIG. 17B

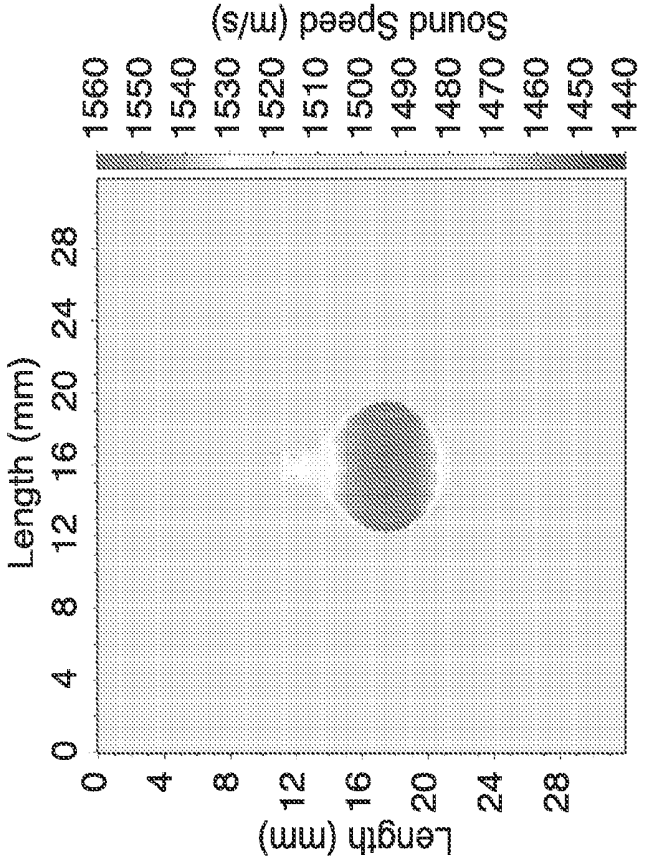

FIG. 17A

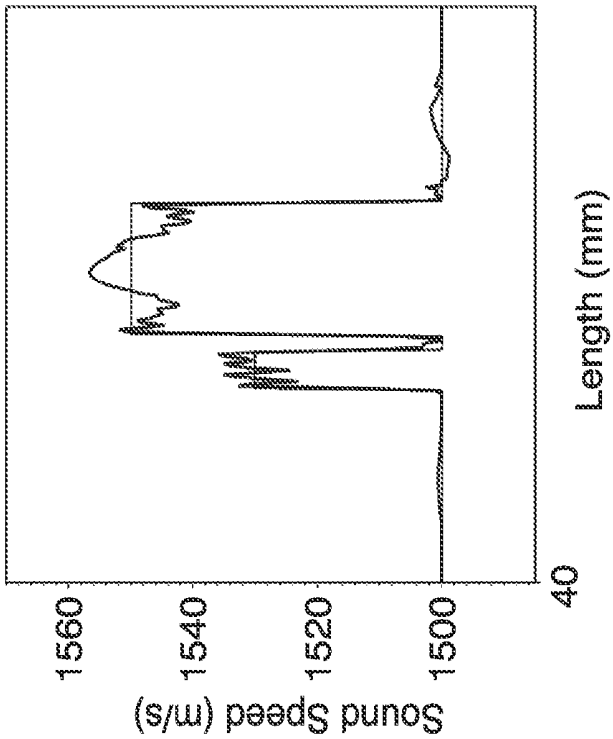

FIG. 18B

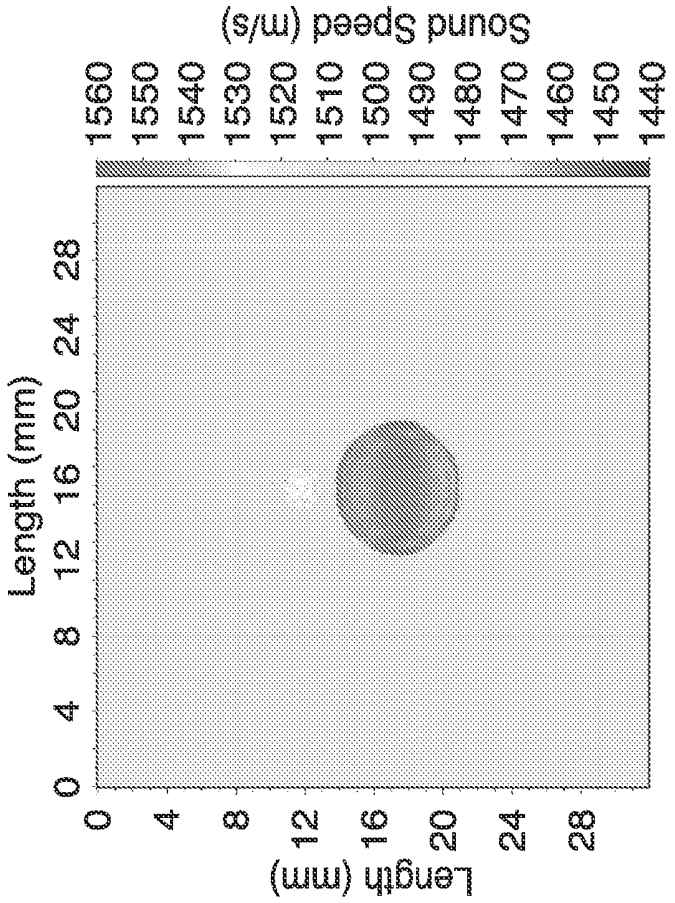

FIG. 18A

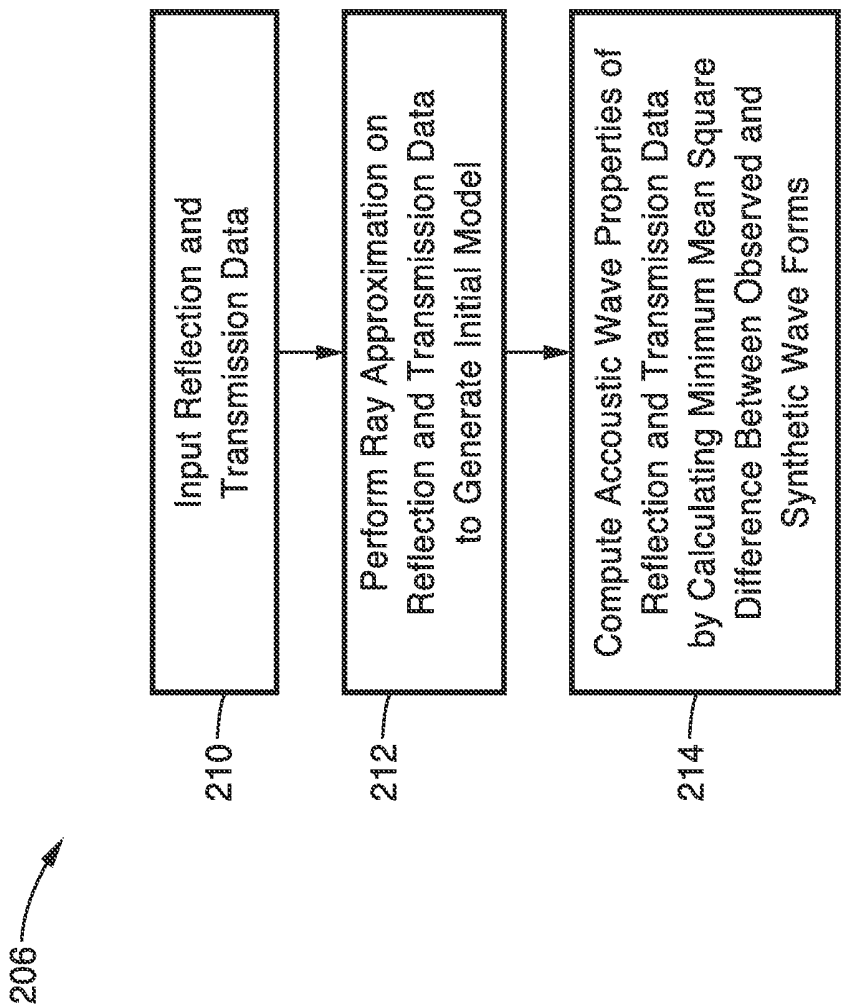
206
Input Reflection and Transmission Data
210
Perform Ray Approximation on Reflection and Transmission Data to Generate Initial Model
212
Compute Accoustic Wave Properties of Reflection and Transmission Data by Calculating Minimum Mean Square Difference Between Observed and Synthetic Wave Forms
214

FIG. 19

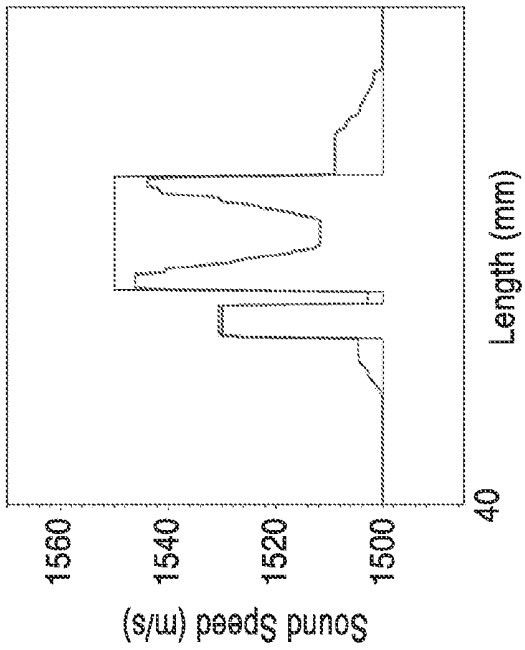

FIG. 20B

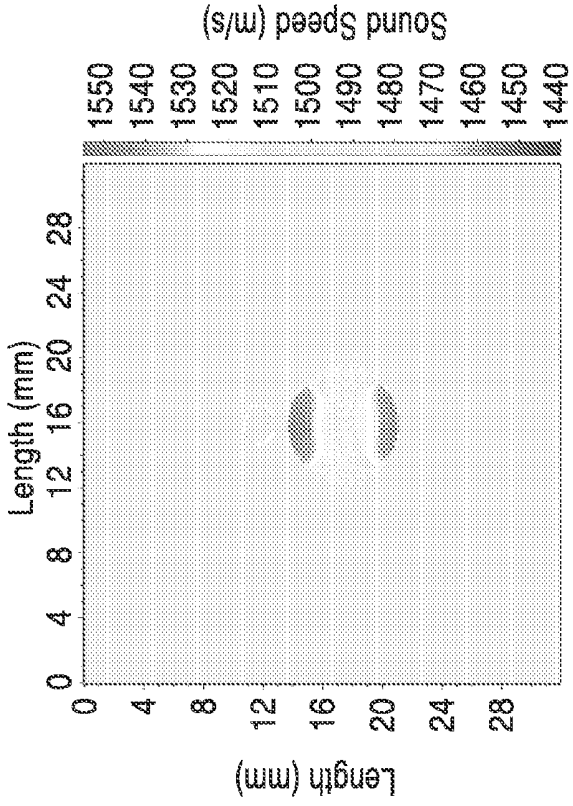

FIG. 20A

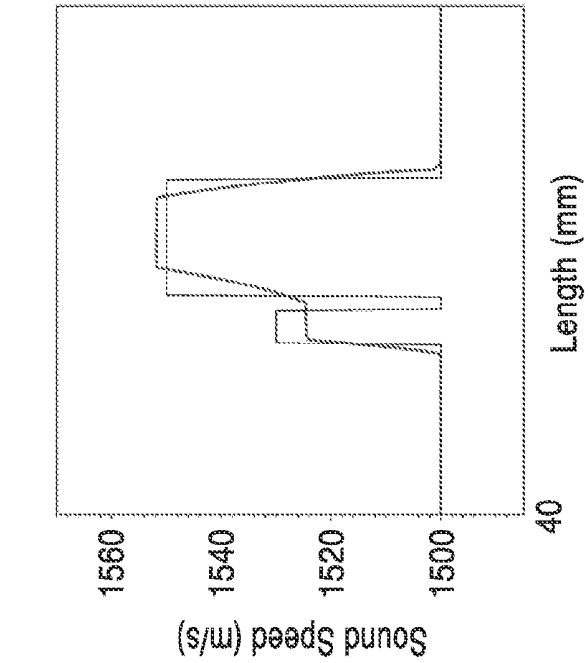

FIG. 21B

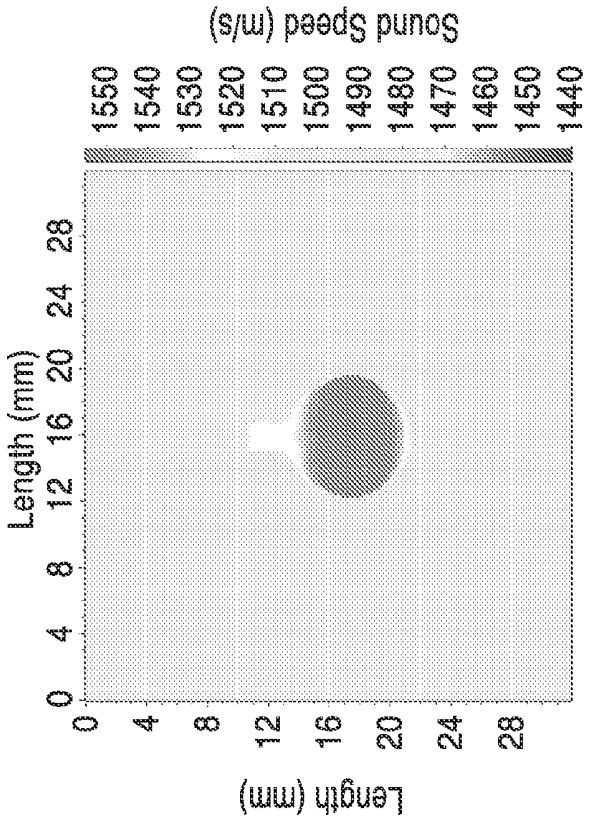

FIG. 21A

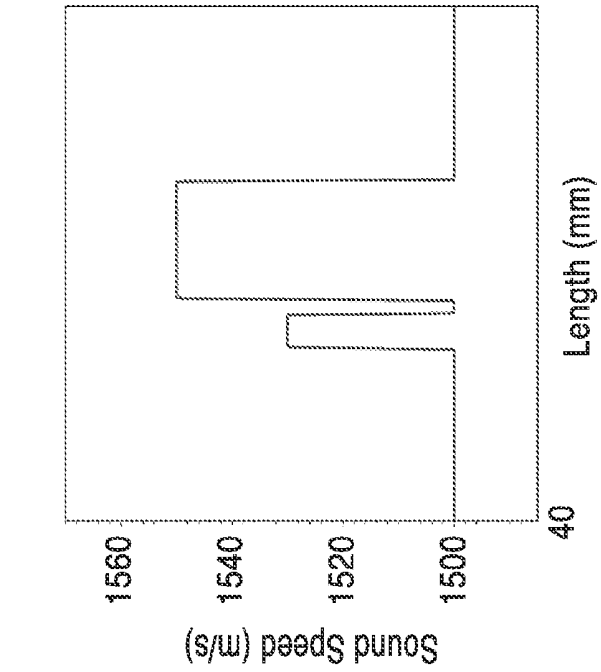

FIG. 22B

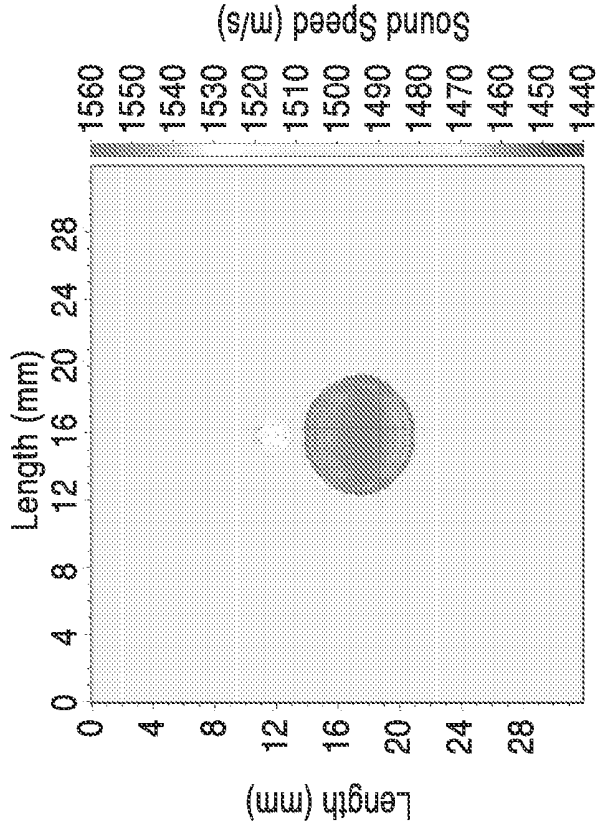

FIG. 22A

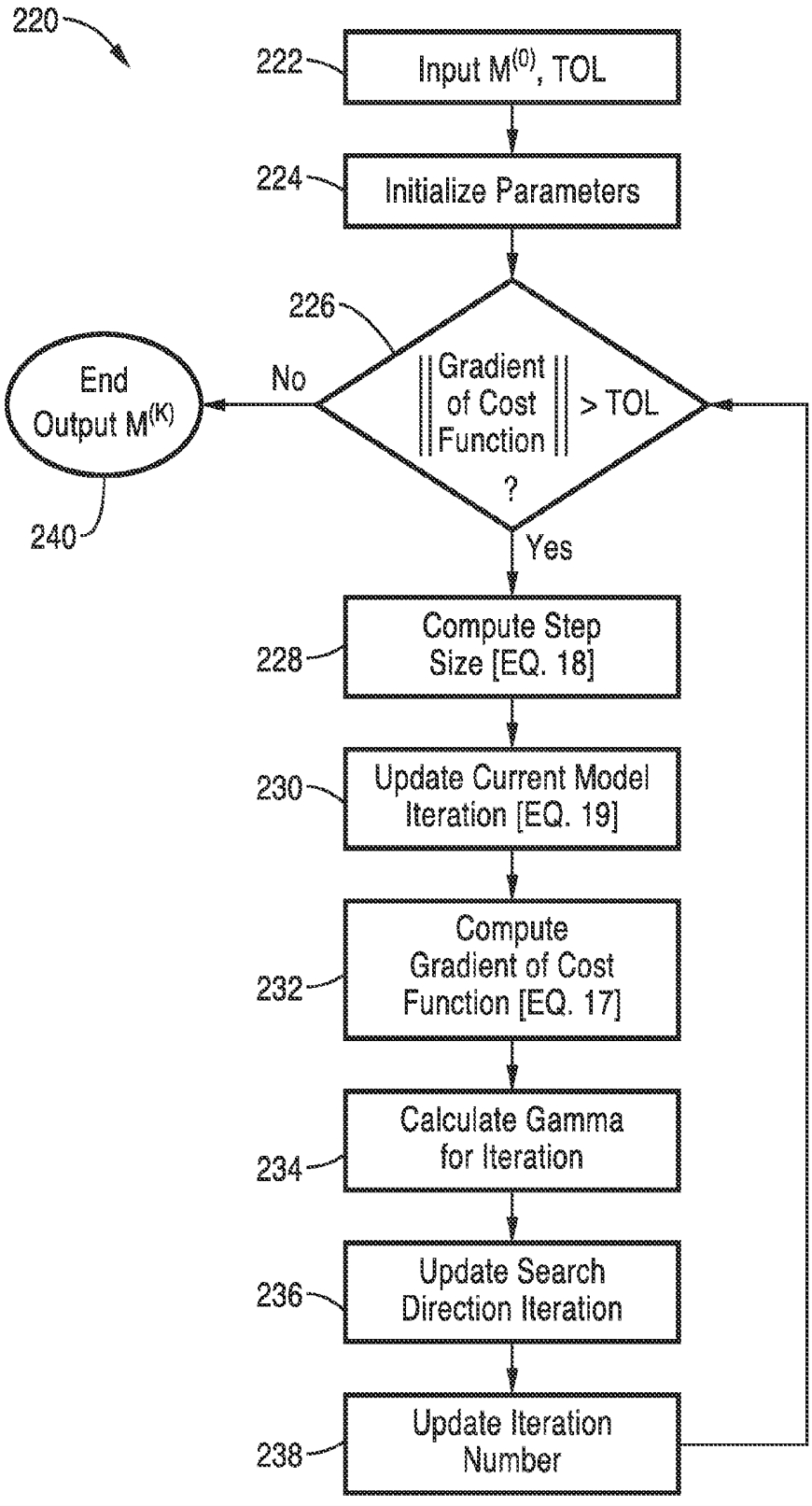
220
222
Input $M^{(0)}$, TOL
224
Initialize Parameters
226
||Gradient of Cost Function|| > TOL ?
No
End
Output $M^{(K)}$
240
Yes
228
Compute Step Size [EQ. 18]
230
Update Current Model Iteration [EQ. 19]
232
Compute Gradient of Cost Function [EQ. 17]
234
Calculate Gamma for Iteration
236
Update Search Direction Iteration
238
Update Iteration Number

FIG. 23

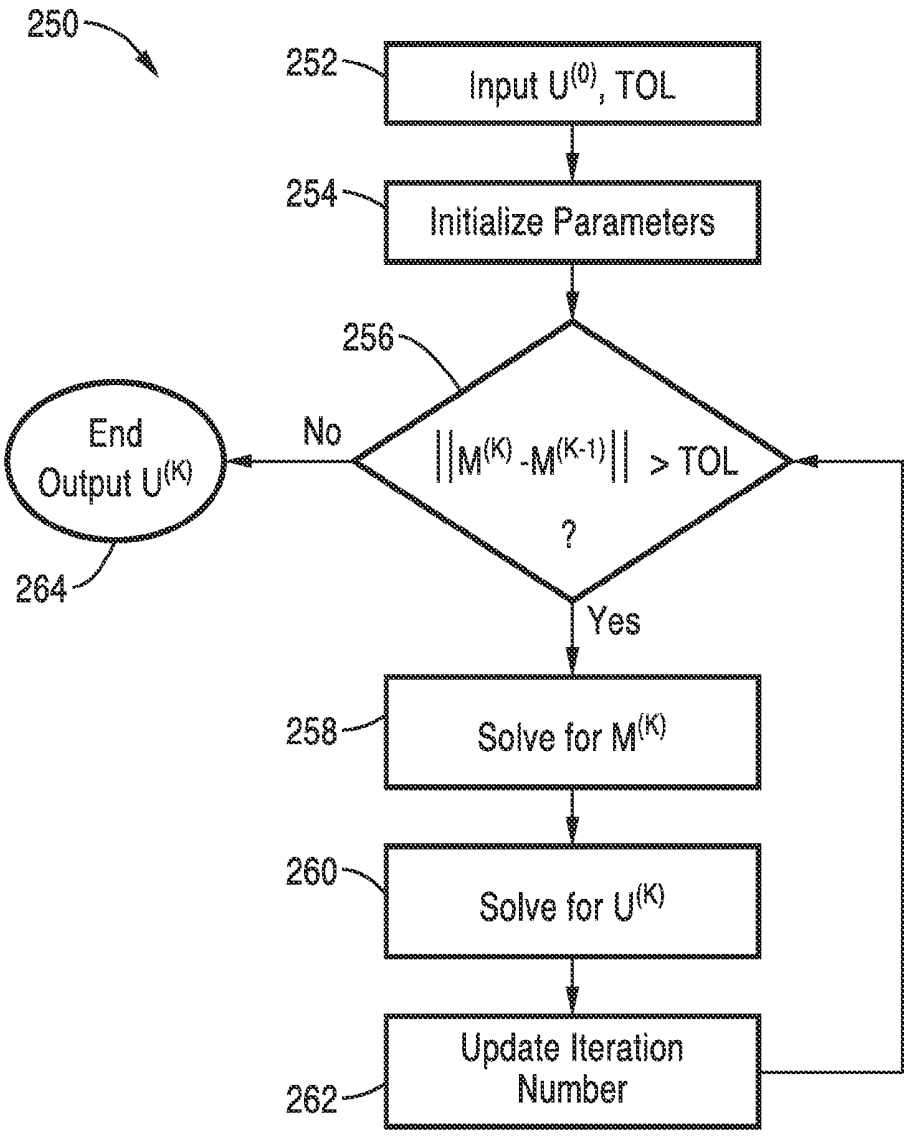
250
252
Input $U^{(0)}$, TOL
254
Initialize Parameters
256
$||M^{(K)} - M^{(K-1)}|| > TOL$?
No
End
Output $U^{(K)}$
264
Yes
258
Solve for $M^{(K)}$
260
Solve for $U^{(K)}$
262
Update Iteration Number

FIG. 24

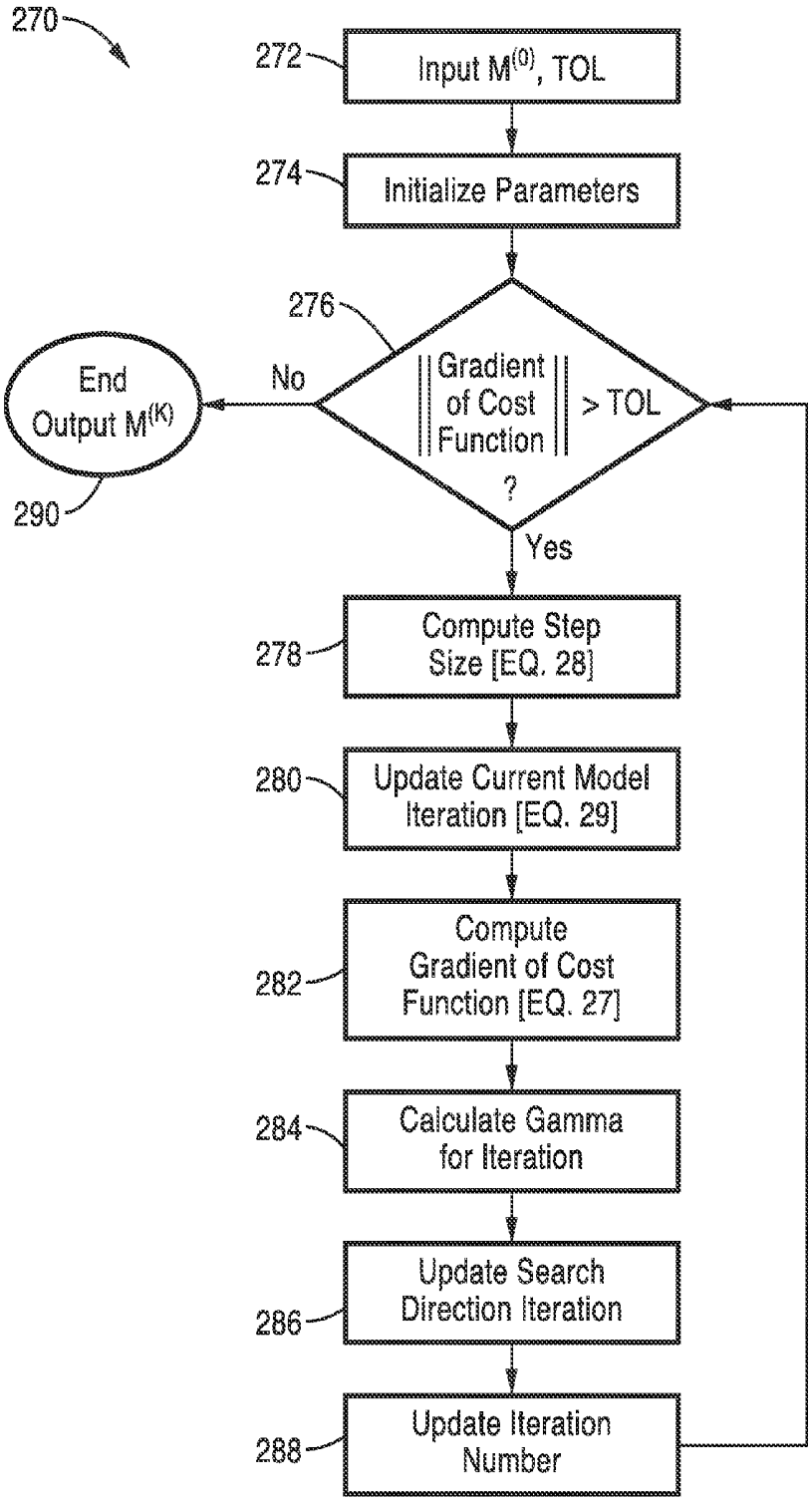
270
272
Input $M^{(0)}$, TOL
274
Initialize Parameters
276
||Gradient of Cost Function|| > TOL ?
No
End
Output $M^{(K)}$
290
Yes
278
Compute Step Size [EQ. 28]
280
Update Current Model Iteration [EQ. 29]
282
Compute Gradient of Cost Function [EQ. 27]
284
Calculate Gamma for Iteration
286
Update Search Direction Iteration
288
Update Iteration Number

FIG. 25

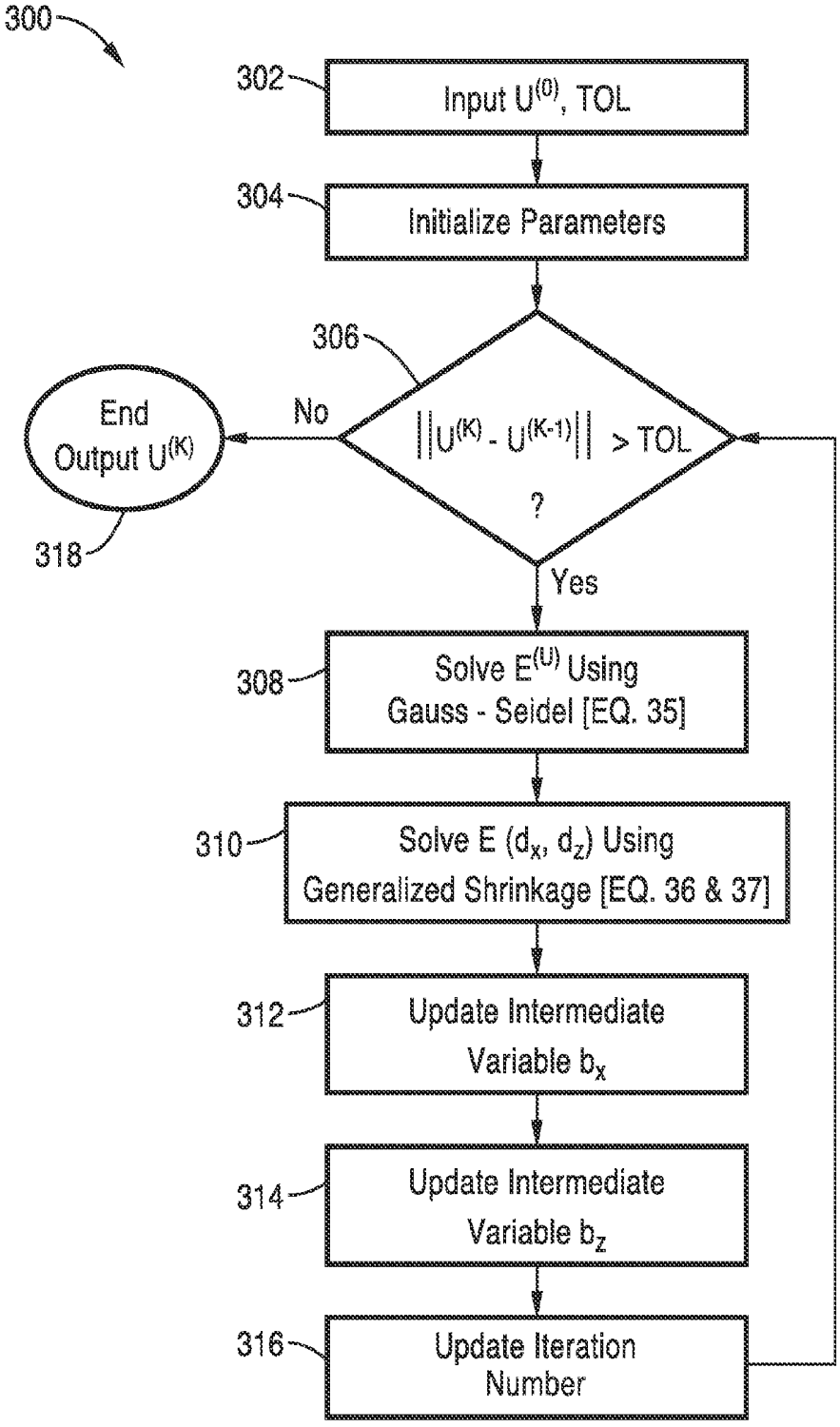
300
302
Input $U^{(0)}$, TOL
304
Initialize Parameters
306
$||U^{(K)} - U^{(K-1)}|| > TOL$
?
No
End
Output $U^{(K)}$
318
Yes
308
Solve $E^{(U)}$ Using
Gauss - Seidel [EQ. 35]
310
Solve E (d_x, d_z) Using
Generalized Shrinkage [EQ. 36 & 37]
312
Update Intermediate
Variable b_x
314
Update Intermediate
Variable b_z
316
Update Iteration
Number

FIG. 26

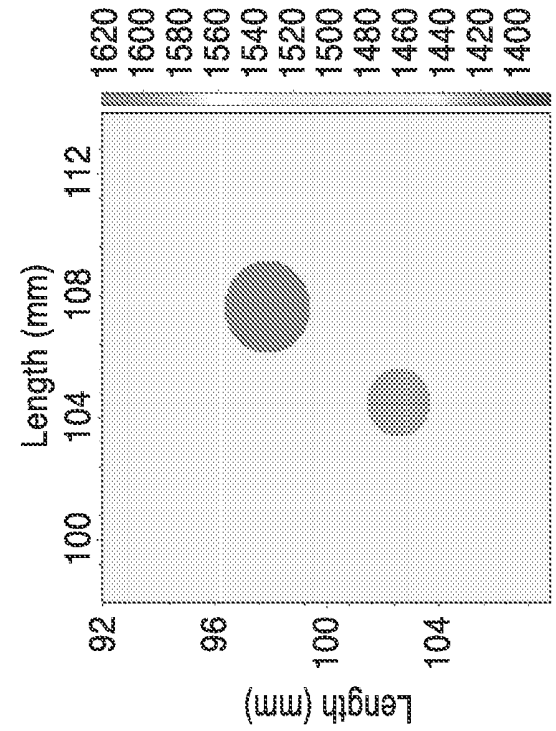

FIG. 27B

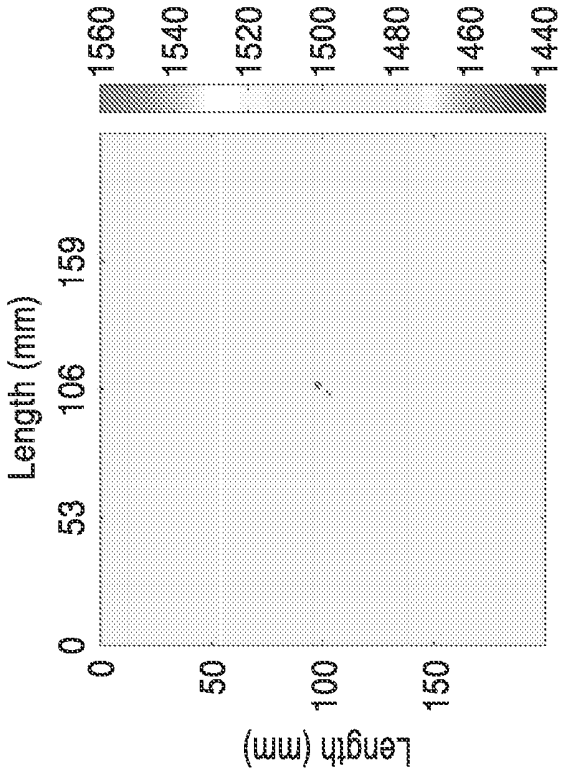

FIG. 27A

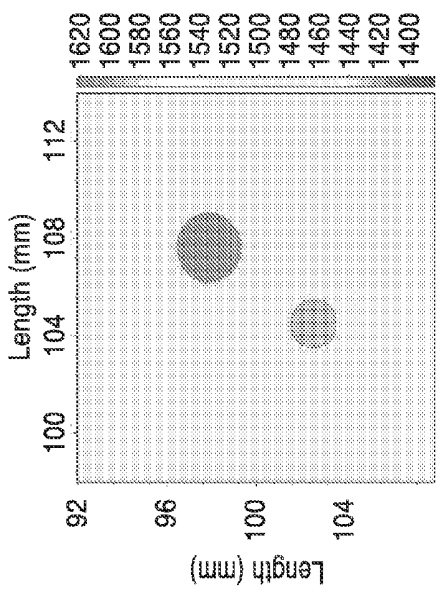

FIG. 28B

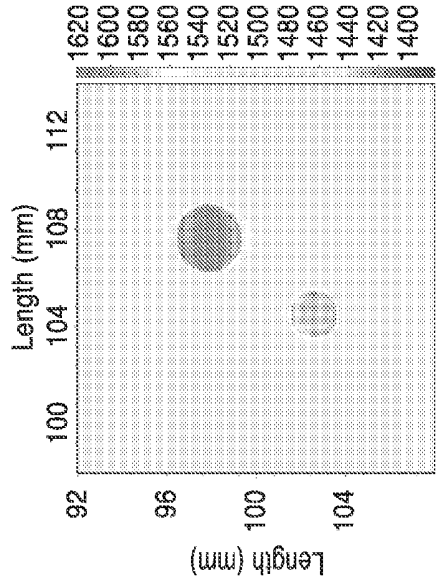

FIG. 28A

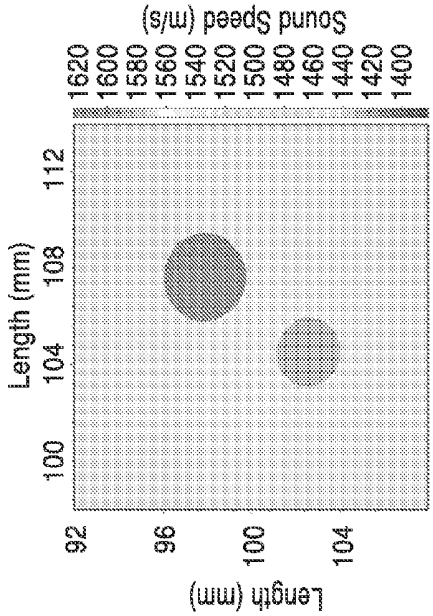

FIG. 28C

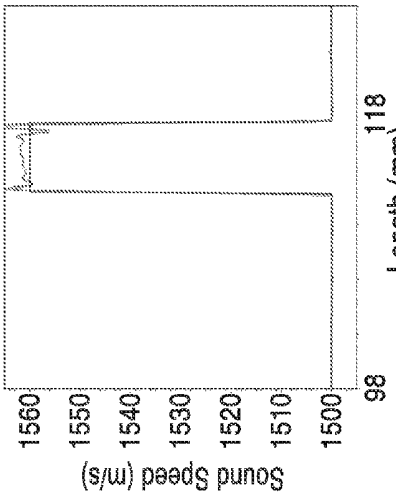

FIG. 29B

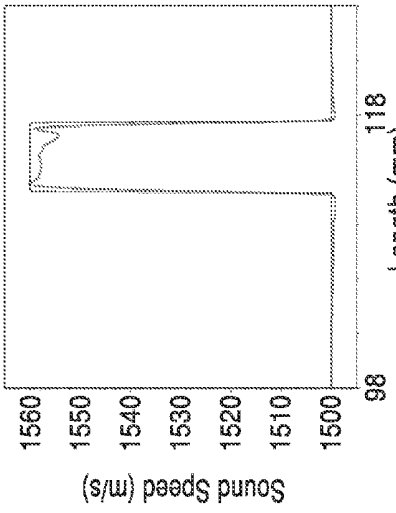

FIG. 29A

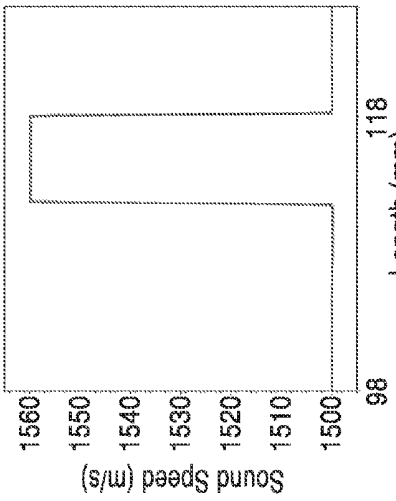

FIG. 29C

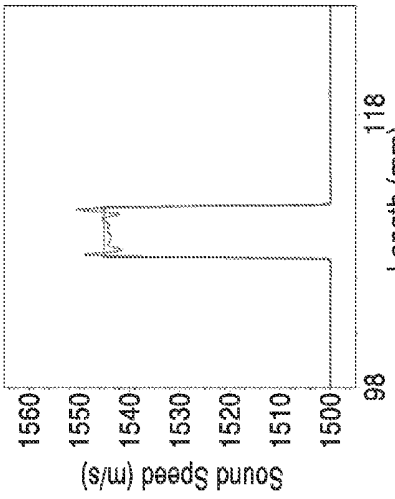

FIG. 30B

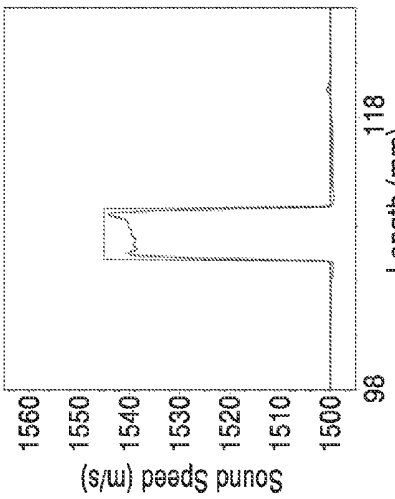

FIG. 30A

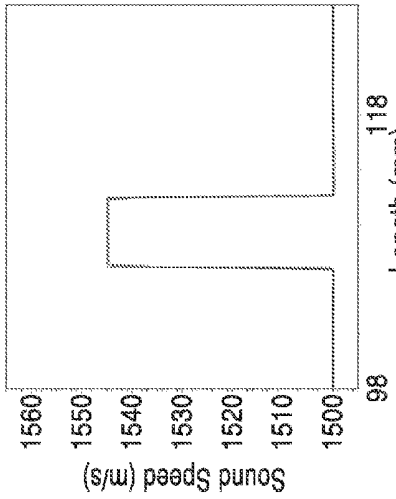

FIG. 30C

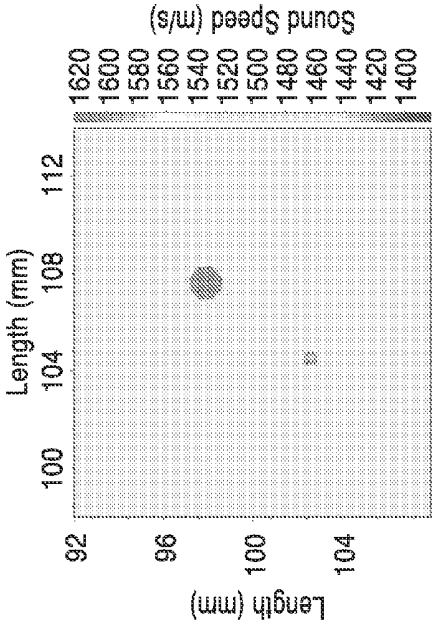

FIG. 31B

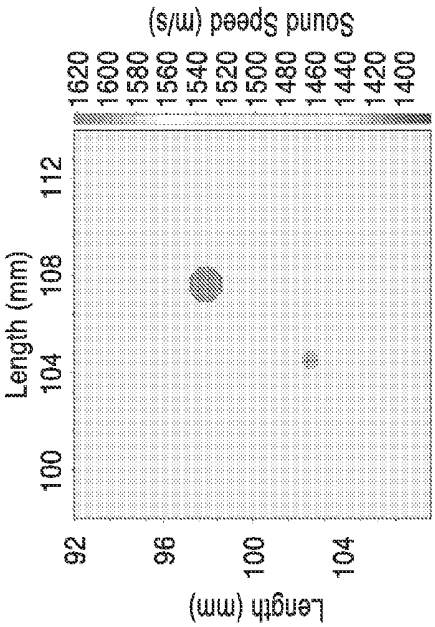

FIG. 31A

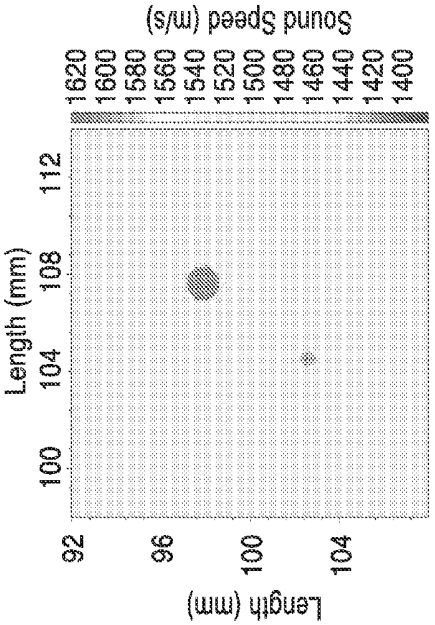

FIG. 31C

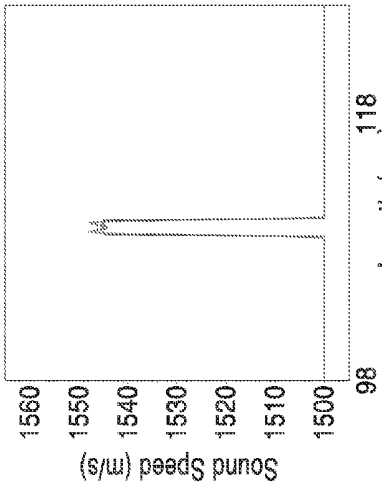

FIG. 32B

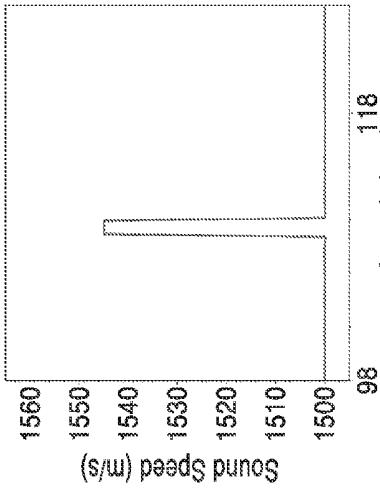

FIG. 32D

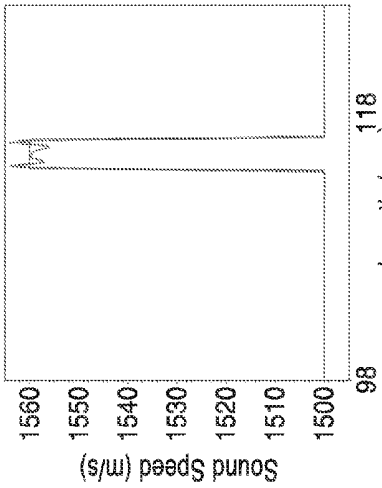

FIG. 32A

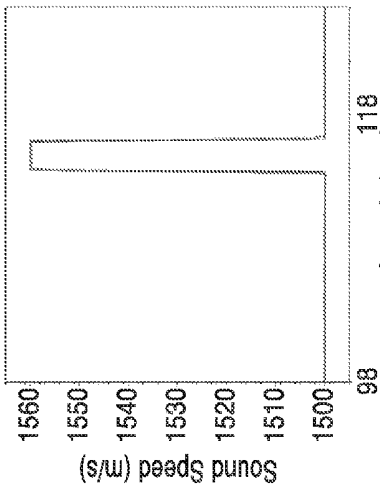

FIG. 32C

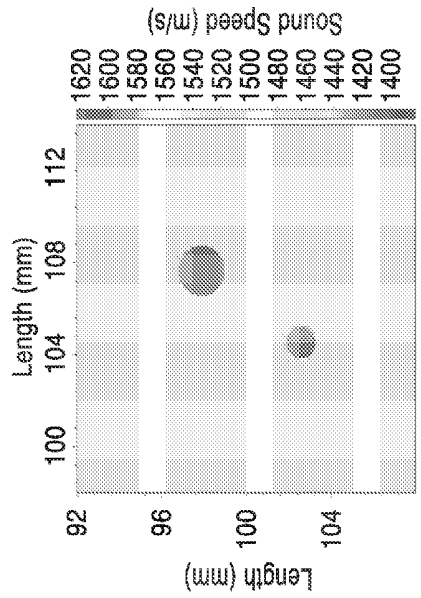

FIG. 33B

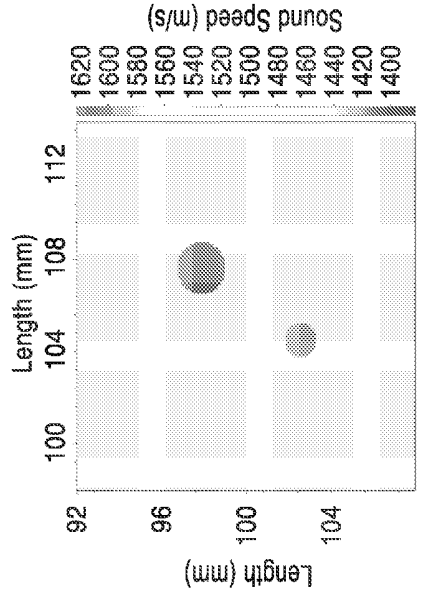

FIG. 33A

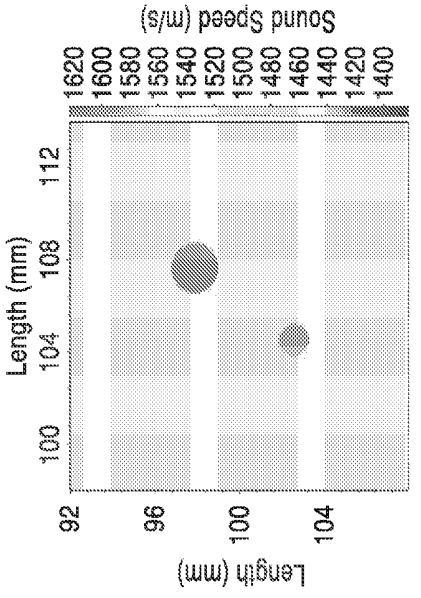

FIG. 33C

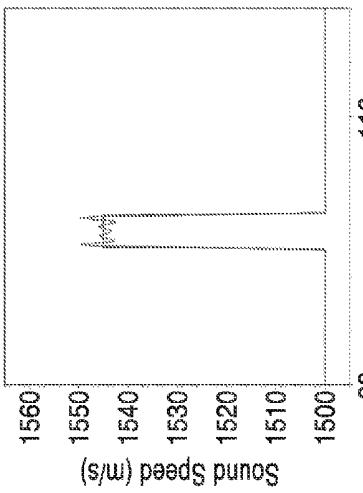

FIG. 34B

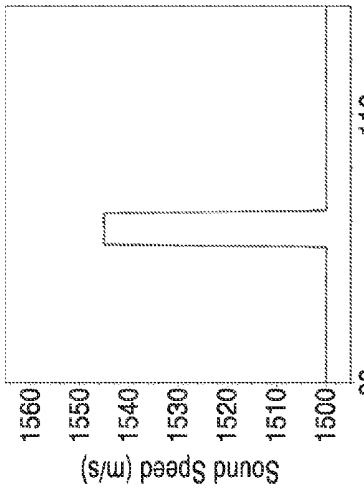

FIG. 34D

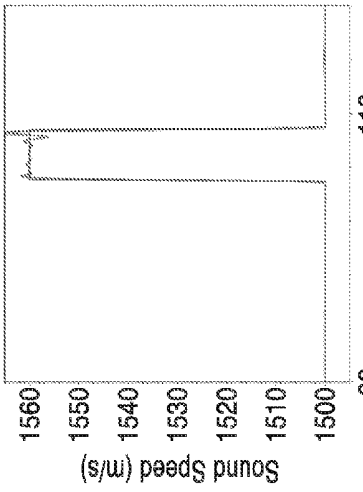

FIG. 34A

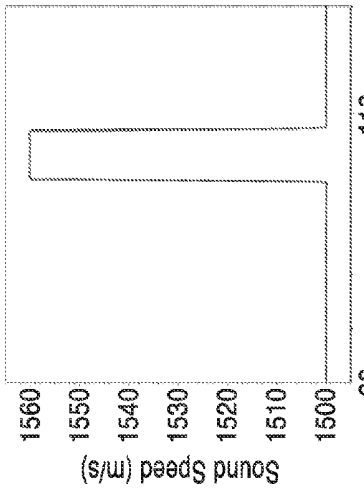

FIG. 34C

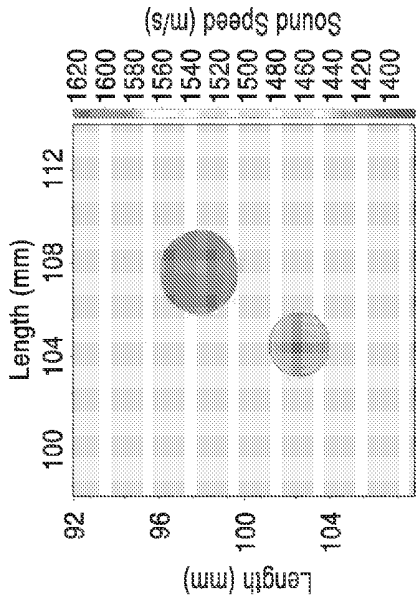

FIG. 35B

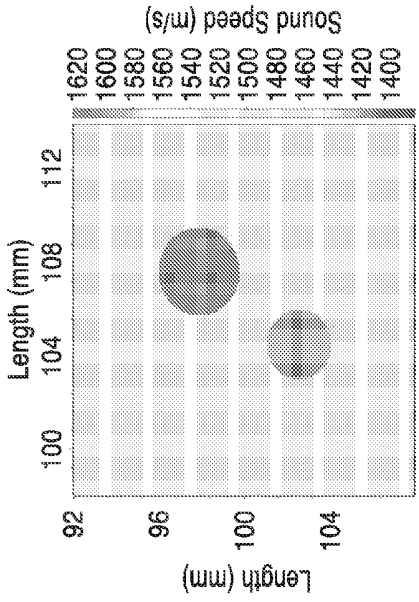

FIG. 35A

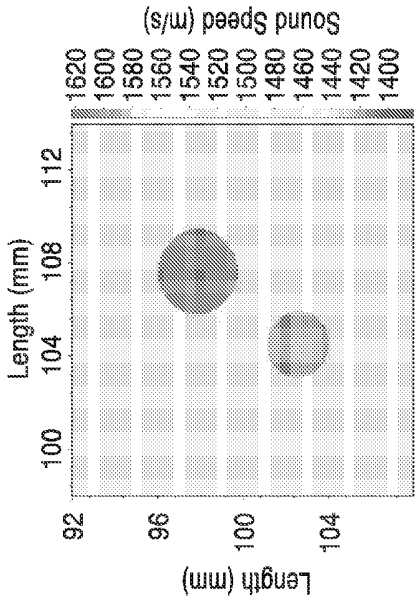

FIG. 35C

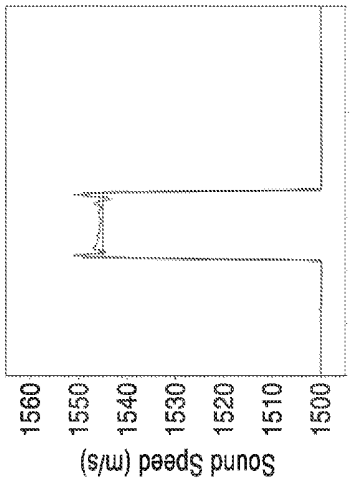

FIG. 36B

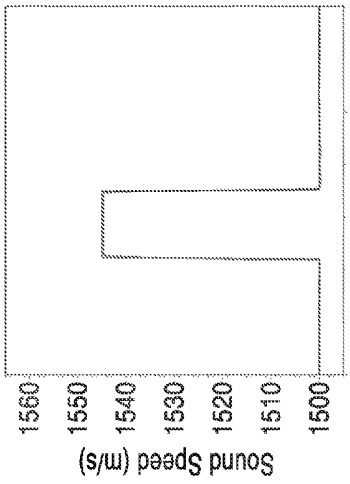

FIG. 36D

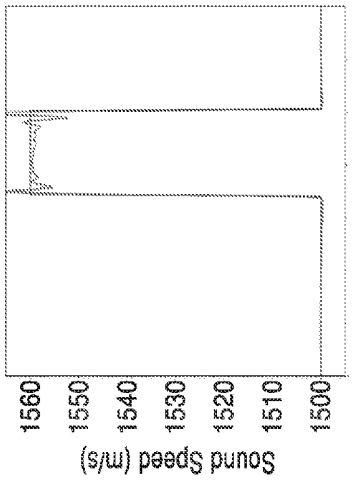

FIG. 36A

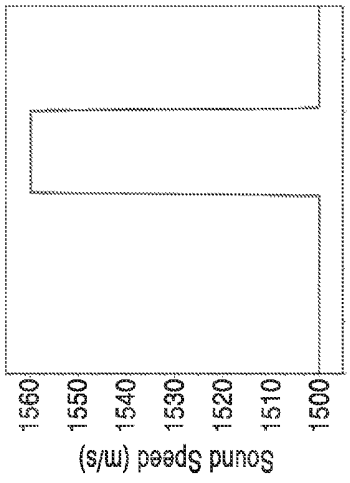

FIG. 36C

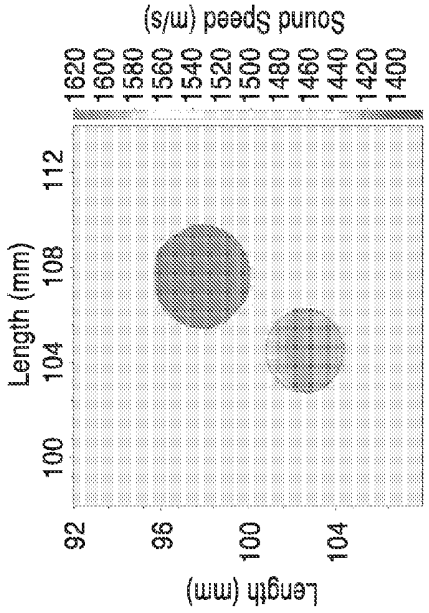

FIG. 37B

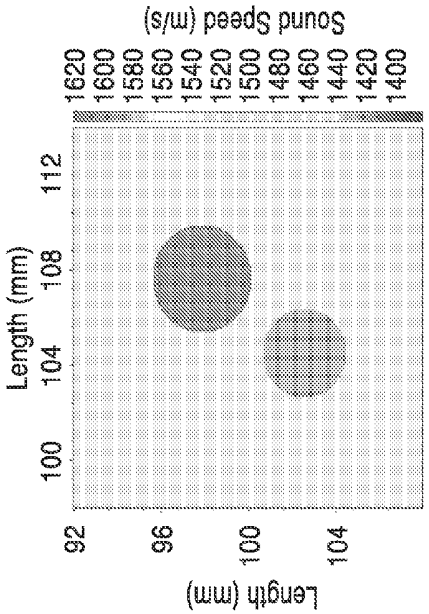

FIG. 37A

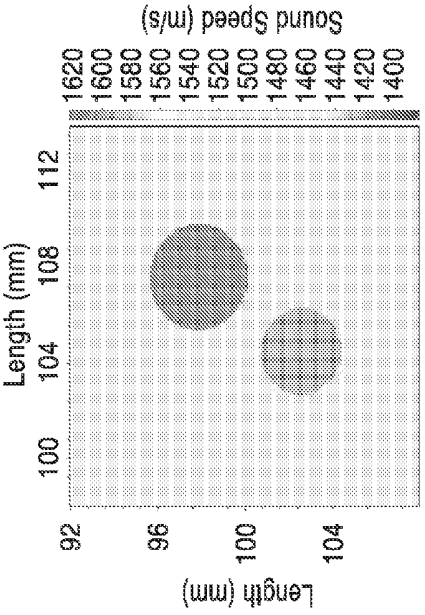

FIG. 37C

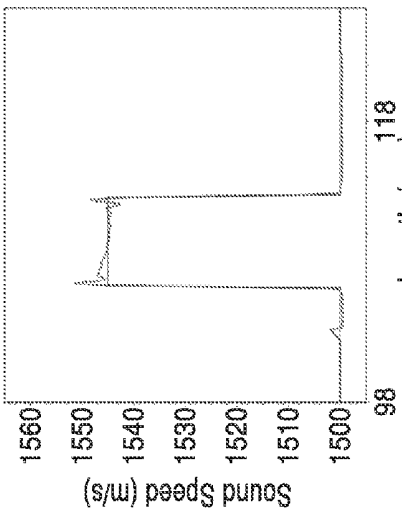

FIG. 38B

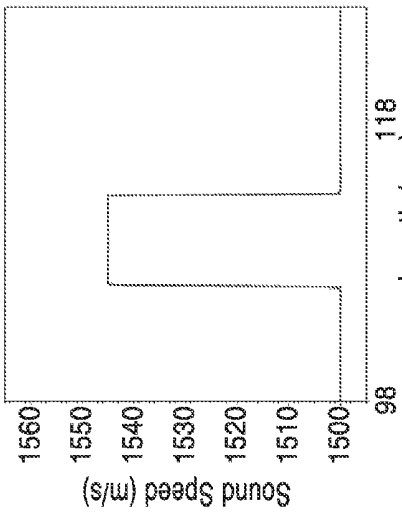

FIG. 38D

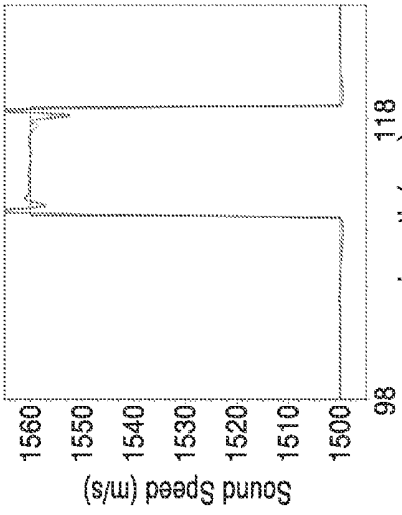

FIG. 38A

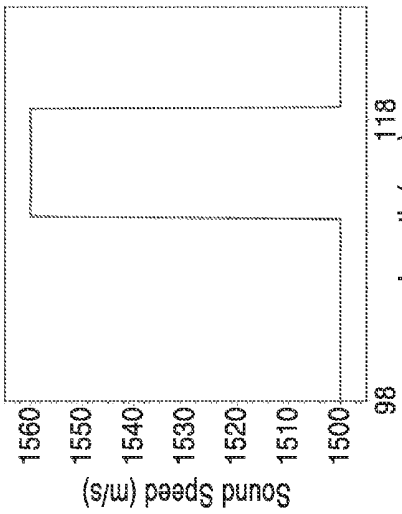

FIG. 38C

ULTRASOUND WAVEFORM TOMOGRAPHY WITH TV REGULARIZATION

CROSS-REFERENCE TO RELATED APPLICATIONS

[0001] This application is a 35 U.S.C. §111(a) continuation of PCT international application number PCT/US2013/024545 filed on Feb. 3, 2013, incorporated herein by reference in its entirety, which claims priority to, and the benefit of, U.S. provisional patent application Ser. No. 61/594,865, filed on Feb. 3, 2012, incorporated herein by reference in its entirety. Priority is claimed to each of the foregoing applications.

[0002] The above-referenced PCT international application was published as PCT International Publication No. WO 2013/116809 on Aug. 8, 2013, incorporated herein by reference in its entirety.

STATEMENT REGARDING FEDERALLY SPONSORED RESEARCH OR DEVELOPMENT

[0003] This invention was made with Government support under Contract No. DE-AC52-06NA25396 awarded by the Department of Energy. The Government has certain rights in the invention.

INCORPORATION-BY-REFERENCE OF COMPUTER PROGRAM APPENDIX

[0004] Not Applicable

NOTICE OF MATERIAL SUBJECT TO COPYRIGHT PROTECTION

BACKGROUND OF THE INVENTION

[0006] 1. Field of the Invention

[0007] This invention pertains generally to imaging, and more particularly to ultrasound imaging using a synthetic aperture ultrasound ray tomography and ultrasound waveform tomography.

[0008] 2. Description of Related Art

[0009] Breast cancer is the second-leading cause of cancer death among American women. The breast cancer mortality rate in the U.S. has been flat for many decades, and has decreased only about 20% since the 1990s. Early detection is the key to reducing breast cancer mortality. There is an urgent need to improve the efficacy of breast cancer screening. Ultrasound tomography is a promising, quantitative imaging modality for early detection and diagnosis of breast tumors.

[0010] Ultrasound waveform tomography is gaining popularity, but is computationally expensive, even for today's fastest computers. The computational cost increases linearly with the number of transmitting sources.

[0011] Synthetic-aperture ultrasound has great potential to significantly improve medical ultrasound imaging. In a synthetic aperture ultrasound system, ultrasound from each element of a transducer array propagates to the entire imaging domain, and all elements in the transducer array receive scattered signals.

[0012] Many conventional ultrasound systems record only 180° backscattered signals. Others are configured to receive only transmission data from the scanning arrays. Accordingly, these systems suffer from extensive computational costs, insufficient resolution, or both.

[0013] Waveform inversion can be implemented either in the time domain, or in the frequency domain. Because of the ill-posedness caused by the limited data coverage, multiple local-minimum solutions exist, and therefore, certain stabilization numerical techniques need to be incorporated within inversion process to obtain a global-minimum solution. In recent years, many approaches have been developed for this purpose. Regularization techniques can be employed to alleviate the instability of the original problem. Preconditioning approaches can also be used in waveform inversion to create a well-conditioned problem with lower dimensions. In addition, prior information about the model can be introduced to improve the convergence of waveform inversion.

BRIEF SUMMARY OF THE INVENTION

[0014] The system and method of the present invention uses ultrasound data acquired using a synthetic-aperture ultrasound system. The investigational synthetic-aperture ultrasound tomography system of the present invention allows acquisition of each tomographic slice of patient ultrasound data in real time. In the system, each element of the transducer array transmits ultrasound sequentially, and elements in the transducer array simultaneously record ultrasound signals scattered from the tissue after each element is fired. The features of the system and method of the present invention provide a real-time synthetic-aperture system that can be used for patient data acquisition.

[0015] In the synthetic-aperture ultrasound tomography system of the present invention, ultrasound from each element of a transducer array or a virtual source of multiple elements propagates to the entire imaging domain, and all elements in the transducer array receive ultrasound signals reflected/scattered from the imaging region and/or transmitted/scattered through the imaging region. Therefore, the acquired synthetic-aperture ultrasound data contain information of ultrasound reflected/scattered and transmitted from all possible directions from the imaging domain to the transducer array to generate a more accurate, 3-D, high resolution image, while minimizing computational costs of the system.

[0016] One aspect of the invention is an ultrasound waveform tomography method with the total-variation (TV) regularization to improve sound-speed reconstructions of small breast tumors. The nonlinear conjugate gradient (NCG) method is used to solve waveform inversion with the TV regularization. The gradient of the misfit function is obtained using an adjoint state method.

[0017] Another aspect of the invention is a novel ultrasound waveform tomography method with a modified total-variation regularization scheme, in which a separate regularization term is added, such that the edge-preserving can be more effective without adding too much extra computational cost.

[0018] We minimize the misfit function using an alternating minimization algorithm. The cost function is decomposed

with the modified TV regularization into two regularization problems, a L_2-norm-based Tikhonov regularization problem and a L_1-norm-based TV regularization problem. The non-linear conjugate gradient (NCG) approach is used to solve for the first Tikhonov regularization problem. Then, an adjoint state method is used to compute the gradient of the misfit function. The split-Bregman method to is used to solve the second regularization problems. In one embodiment, the use of the split-Bregman method allows for computations that are (a) it is computationally efficient; and (b) the selection of the smoothing parameter in the TV regularization term can be avoided.

[0019] Further aspects of the invention will be brought out in the following portions of the specification, wherein the detailed description is for the purpose of fully disclosing preferred embodiments of the invention without placing limitations thereon.

BRIEF DESCRIPTION OF THE SEVERAL VIEWS OF THE DRAWING(S)

[0020] The invention will be more fully understood by reference to the following drawings which are for illustrative purposes only:

[0021] FIG. **1** is a schematic diagram of a synthetic-aperture ultrasound system in accordance with the present invention.

[0022] FIG. **2** is a schematic diagram of a synthetic-aperture ultrasound tomography system for scanning breast tissue in accordance with the present invention

[0023] FIG. **3** is a schematic diagram of the scanner of the ultrasound tomography system of FIG. **1** interrogating a region of tissue.

[0024] FIG. **4** shows flow diagram of a method for sequentially exciting a region of tissue and acquiring reflection and transmission data in accordance with the present invention.

[0025] FIG. **5** illustrates a schematic view of a two parallel-bar ultrasound transducer array scanner.

[0026] FIG. **6** illustrates a schematic view of a scanner comprising two parallel planar arrays.

[0027] FIG. **7** shows a schematic view of a cylindrical array scanner having a cylindral 2-D array of transducers and a 2-D planner array at the bottom of the cylinder.

[0028] FIG. **8** shows a flat transducer configured to generate a collimated beam.

[0029] FIG. **9** shows an arcuate transducer configured to generate a diverging beam.

[0030] FIG. **10** shows a schematic view of a torroidal array scanner having a a circular array of transducers.

[0031] FIG. **11** shows a schematic view of a synthetic-aperture ultrasound breast tomography scanner that incorporates use of two circular transducer arrays.

[0032] FIG. **12** shows a schematic view of a scanner comprising a semicircular or arcuate array having transducers in an opposing or facing orientation with planar array.

[0033] FIG. **13** illustrates a scanner that reduces the 2D arrays in FIG. **12** to 1D arrays.

[0034] FIG. **14** is a flow diagram of a synthetic aperture ultrasound tomography method in accordance with the present invention.

[0035] FIG. **15** shows an image of a numerical breast phantom containing two different tumors.

[0036] FIG. **16**A and FIG. **16**B show imaging results (tomographic reconstruction in FIG. **16**A, and vertical profile along the center of the tumors in FIG. **16**B) obtained using only the reflection data.

[0037] FIG. **17**A and FIG. **17**B show imaging results (tomographic reconstruction in FIG. **17**A, and vertical profile along the center of the tumors in FIG. **17**B) obtained using only the transmission data.

[0038] FIG. **18**A and FIG. **18**B show imaging results (tomographic reconstruction in FIG. **18**A, and vertical profile along the center of the tumors in FIG. **18**B) obtained using both transmission and reflection data simultaneously in accordance with method of the present invention.

[0039] FIG. **19** illustrates a method for generating the ultrasound waveform step of FIG. **14** using both transmission and reflection data for ultrasound waveform tomography.

[0040] FIG. **20**A through FIG. **20**B show tomographic reconstruction results for tomographic reconstruction with a modified total-variation regularization scheme using only reflection data.

[0041] FIG. **21**A through FIG. **21**B show results for tomographic reconstruction with a modified total-variation regularization scheme obtained using only transmission data.

[0042] FIG. **22**A through FIG. **22**B show results for tomographic reconstruction with a modified total-variation regularization scheme obtained using both transmission and reflection data in accordance with the present invention.

[0043] FIG. **23** shows a flow diagram for a computational method for solving the TV regularization problem of the present invention.

[0044] FIG. **24** shows a flow diagram for a computational method for solving the modified TV regularization problem of the present invention.

[0045] FIG. **25** shows an algorithm using NCG to solve a step in the method of FIG. **24**.

[0046] FIG. **26** shows an algorithm using Split Bregman iteration to solve a step in the method of FIG. **24**.

[0047] FIG. **27**A and FIG. **27**B are images showing a numerical breast phantom containing two small breast tumors.

[0048] FIG. **28**A through FIG. **28**C show sound-speed reconstructions obtained using ultrasound waveform tomography with (FIG. **28**A) Tikhonov regularization, (FIG. **28**B) TV regularization, and (FIG. **28**C) modified TV regularization.

[0049] FIG. **29**A through FIG. **29**C show horizontal profiles of the waveform tomography reconstructions through the center of the large tumor with (FIG. **29**A) Tikhonov regularization, (FIG. **29**B) TV regularization, and (FIG. **29**C) modified TV regularization.

[0050] FIG. **30**A through FIG. **30**C show horizontal profiles of the waveform tomography reconstructions through the center of a small tumor with (FIG. **30**A) Tikhonov regularization, (FIG. **30**B) TV regularization, and (FIG. **30**C) modified TV regularization.

[0051] FIG. **31**A through FIG. **31**C show images of numerical breast phantom FIG. **31**A containing two tumors with sizes of 0.75 mm (half a wavelength) and 1.5 mm (1 wavelength), TV reconstruction (FIG. **31**B), along with modified TV reconstruction (FIG. **31**C).

[0052] FIG. **32**A and FIG. **32**B are images showing horizontal profiles of the result of ultrasound waveform tomog-

raphy with TV regularization through the center of the large tumor (FIG. **32**A), and through the center of the small tumor (FIG. **32**B).

[0053] FIG. **32**C and FIG. **32**D are images showing horizontal profiles of the result of ultrasound waveform tomography with modified TV regularization through the center of the large tumor (FIG. **32**C), and through the center of the small tumor (FIG. **32**D).

[0054] FIG. **33**A through FIG. **33**C show images of numerical breast phantom (FIG. **33**A) containing two tumors with sizes of 1.5 mm (1 wavelength) and 2.25 mm (1.5 wavelengths), TV reconstruction (FIG. **33**B), along with modified TV reconstruction (FIG. **33**C).

[0055] FIG. **34**A and FIG. **34**B are images showing horizontal profiles of the result of ultrasound waveform tomography with TV regularization through the center of the large tumor (FIG. **34**A), and through the center of the small tumor (FIG. **34**B).

[0056] FIG. **34**C and FIG. **34**D are images showing horizontal profiles of the result of ultrasound waveform tomography with modified TV regularization through the center of the large tumor (FIG. **34**C), and through the center of the small tumor (FIG. **34**D).

[0057] FIG. **35**A through FIG. **35**C show images of numerical breast phantom FIG. **35**A containing two tumors with sizes of 3.0 mm (2 wavelengths) and 3.75 mm (2.5 wavelengths), TV reconstruction (FIG. **35**B), along with modified TV reconstruction (FIG. **35**C).

[0058] FIG. **36**A and FIG. **36**B are images showing horizontal profiles of the result of ultrasound waveform tomography with TV regularization through the center of the large tumor (FIG. **36**A), and through the center of the small tumor (FIG. **36**B).

[0059] FIG. **36**C and FIG. **36**D are images showing horizontal profiles of the result of ultrasound waveform tomography with modified TV regularization through the center of the large tumor (FIG. **36**C), and through the center of the small tumor (FIG. **36**D).

[0060] FIG. **37**A through FIG. **37**C show images of numerical breast phantom FIG. **37**A containing two tumors with sizes of 3.75 mm (2.5 wavelengths) and 4.5 mm (3 wavelengths), TV reconstruction (FIG. **37**B), along with modified TV reconstruction (FIG. **37**C).

[0061] FIG. **38**A and FIG. **38**B are images showing horizontal profiles of the result of ultrasound waveform tomography with TV regularization through the center of the large tumor (FIG. **38**A), and through the center of the small tumor (FIG. **38**B).

[0062] FIG. **38**C and FIG. **38**D are images showing horizontal profiles of the result of ultrasound waveform tomography with modified TV regularization through the center of the large tumor (FIG. **38**C), and through the center of the small tumor (FIG. **38**D).

DETAILED DESCRIPTION OF THE INVENTION

[0063] The description below is directed to synthetic aperture ultrasound tomography systems for imaging a medium such as patient tissue, along with ultrasound waveform tomography methods for acquiring and processing data acquired from these systems, or other systems that may or may not be available in the art.

[0064] The synthetic-aperture breast ultrasound tomography system of the present invention uses synthetic-aperture ultrasound to obtain quantitative values of mechanical properties of breast tissues. In this system, each transducer element transmits ultrasound waves sequentially, and when an ultrasound transducer element transmits ultrasound waves propagating through the breast, all ultrasound transducer elements (at least within a portion of an array) simultaneously receive ultrasound reflection/transmission, or forward and backward scattering signals. The ultrasound reflection/transmission signals are used to obtain quantitative values of mechanical properties of tissue features (and in particular breast tumors), including the sound speed, density, and attenuation.

[0065] While the systems and methods described below are particularly directed and illustrated for imaging of breast tissues, it is appreciated that the systems and methods may also be employed for waveform tomography on other tissues or scanning mediums.

[0066] I. Synthetic Aperture Ultrasound Tomography System

[0067] FIG. **1** is a schematic diagram of a synthetic-aperture ultrasound system **10** in accordance with the present invention. The system **10** includes a scanner **12** comprising a plurality of individual transducer elements **16** disposed within one or more arrays (e.g. the opposing parallel arrays **14***a* and **14***b* shown in FIG. **1**). The scanner **12** is coupled to a server or like computing apparatus **20** (e.g. with a cable **15** or other connection means such as, but not limited to, a wireless connections means) and synthetic aperture ultrasound data acquisition system **18** that outputs RF data **28** corresponding to readings acquired by the scanner **12**.

[0068] The computer **20** comprises a processor **24** configured to operate one or more application programs **22** located within memory **25**, wherein the application programs **22** may contain one or more algorithms or methods of the present invention for imaging a tissue medium for display via a graphical user interface **23** on monitor **26**, or other means. For example, the application programming **22** may comprise the programming configured for operating the sequential excitation method **50** shown in FIG. **4** or ultrasound waveform tomography imaging method **200** shown in FIG. **14**. The computer **20** controls ultrasound tomography data acquisition, and the process is completed automatically. The whole-breast scanning time with approximately 100 slides takes approximately 2 minutes.

[0069] FIG. **2** is a schematic view of a breast ultrasound tomography system **11** in accordance with the present invention. System **11** includes a table **70** having a water tank **76** with an open aperture at the top of the table **70** for insertion of the patient's breast tissue (which ideally hangs pendant within water tank **76** during imaging). Tank **76** includes one or more synthetic-aperture ultrasound transducer arrays **74** located within one or more surfaces of the tank. The transducer array(s) **74** are immersed within the water tank **76** configured for receiving the patients breast **44** through aperture **72**, and scanning the breast **44** while the patient is lying down on the table **70** in the prone position. As described in further detail below, transducer array(s) **74** may comprise a number of different configurations, with the water tank housing **76** shaped accordingly to house the array(s) **74**. The water tank housing **76** material preferably comprises a light, non-conductive material that conforms to the shape of the array(s) **74** (e.g. rectangular for 2-parallel bar array scanner **12** of FIG. **1**, or cylindrical for the scanners **110**, **120** and **130** shown in FIG. **7**, FIG. **10** and FIG. **11**, respectively).

[0070] Positioning of the active areas of all array(s) **74** relative to the water tank housing **76** is preferrably aligned such that the ultrasound energy for the transducer elements **16** (FIG. **1**) is focused onto the same plane perpendicular to the housing (for parallel bar scanner **12** (FIG. **5**) or planar **100** (FIG. **6**) arrays). The arrays (e.g. arrays **14***a* and **14***b*, FIG. **1**) are preferrably electrically isolated and grounded.

[0071] The system **11** includes a data acquisition system **18** that may be coupled to a computer system or electronics **78** that control scanning. The data acquisition system **18** may also be coupled to a computer **20** for running application programming **22** (FIG. **1**) to perform tomography reconstructions.

[0072] During the ultrasound data acquisition in the synthetic-aperture ultrasound tomography system **10**, the raw ultrasound data **28** (radio-frequency data) may be first stored within computer memory **25** (FIG. **1**) (which may comprise solid state drives or other storage means available in the art), allowing real-time patient data acquisition for clinical applications.

[0073] FIG. **3** is a schematic diagram of the two parallel bar arrays **14***a* and **14***b* of scanner **12** of FIG. **1** shown interrogating a region of tissue **44** (e.g. breast tissue for mammography) in accordance with a preferred method of the present invention. The ultrasound imaging system **10** focuses an array **14***a* and **14***b* of N transducers **16** acting in a transmit-receive mode. Each element of the array **14***a* **14***b* is excited sequentially (e.g. transducer **3** of array **14***a* is shown in excitation mode) to generate an ultrasound field or signal **30** through the tissue surface **40** and into tissue medium **44** having a plurality of point scatterers **42**. The backscattered signals **32** are measured in parallel by all N elements **16**. In addition, opposing array **14***b* transducers are positioned facing array **14***a* such that one or more elements of the array **14***b* receive direct transmission signals **30** simultaneously with reception of backscatter or reflection signals **32** being received by array **14***a*.

[0074] FIG. **4** shows flow diagram of a method **50** for sequentially exciting a region of tissue **44** in accordance with the present invention. At step **52**, a first element (e.g. element **1** or i) of array **14***a* **14***b* of N ultrasound transducer elements **16** is excited for interrogating an inhomogeneous medium **44**. At step **54**, the backscattered/reflected signals **32** are received/measured by all elements **16** (of at least **14***a*), while transmission signals **30** are received/measured by one or more elements **16** of array **14***b*. At step **58**, the method evaluates whether all the elements **16** in the arrays **14***a* and **14***b* have been excited (and imaged). If the last element in the arrays **14***a*, **14***b* has not been reached, the method moves to the next element **16** in the array (**14***a* or **14***b*) at step **60**, and repeats the process sequentially until the N^{th} element is reached. At this point, the individual reflection/transmission data are RF data, and the process **50** transfers the RF data to memory or solid state drives **25** at step **64**.

[0075] In the phased transducer arrays for synthetic-aperture breast ultrasound tomography, a plurality of transducer elements **16** are fired with different delayed times to simulate ultrasound waves emerging from a virtual point source. The systems and methods of the present invention preferrably use the virtual point sources of the synthetic-aperture breast ultrasound tomography system to improve signal-to-noise ratios of breast ultrasound data.

[0076] The various scanning arrays invention, described below with reference to FIG. **5** through FIG. **7** and FIG. **10** through FIG. **13**, are shown to illustrate that the systems **10**, **11** and methods **50**, **200** may be achieved in various configurations. Yet, the scanning arrays of FIG. **5** through FIG. **7** and FIG. **10** through FIG. **13** all share at least one common characteristic in that at a plurality of transducers **16** of an array, or portion of an array, oppose (at a spaced-apart distance across the target scanning medium **44**) a plurality of transducers **16** of either another portion of the array, or a separate array, so that reflection and transmission data may be acquired with each successive transducer excitation. The following are specific examples of arrays that may be used in the systems **10**, **11** and methods **50**, **200** of the present invention. However, other configurations are contemplated. In each of these configurations, the scanner **74** is shown without table **70** or housing **76** for clarity.

[0077] A. Dual Parallel-Bar Array Scanner

[0078] FIG. **5** illustrates a two parallel-bar ultrasound transducer array scanner **12**, which is illustrated in reference to implementation within system **10** in FIG. **1**, and schematically in operation as a synthetic-aperture scanner in FIG. **3**.

[0079] As shown in FIG. **5**, the two arrays **14***a* and **14***b* are shown in opposing orientation (e.g facing eachother and matching in location along x-axis in FIG. **5**), and positioned in the x-y plane (preferrably parallel to table **70** in FIG. **2**, such that they are spaced-apart across the scanning region **44**. Each of the **14***a* and **14***b* comprises a plurality of N transducers **16** (e.g. count of 128) linearly aligned in series (shown in along the x-axis for reference) as parallel-phased arrays firing toward each other in operation (see FIG. **3**).

[0080] A robotic stage **90** is provided so that the arrays can move in unison vertically along the z-axis to scan the tissue **44**. The transducer arrays **14***a* and **14***b* are configured to scan the breast **44** from the chest wall to the nipple region, slice by slice. To image the axillary region (region of breast closest to the armpit of the patient, not shown), the two transducer arrays **14***a* and **14***b* can be steered toward the axillary region, with one of the transducer arrays placed near the axillary region. The axillary region, or basin, is important to oncologic surgeons, as it represents the principal lymphatic drainage region of the breast. Lymphatic metastasis from a malignant breast lesion will most often occur in this region.

[0081] Arrays **14***a* and **14***b* may also be translated (either in concert, or with respect to each other) in the x and y axes to closely conform to varying patient anatomy.

[0082] Referring to FIG. **8** and FIG. **9**, the transducer **16** may either be flat or circular, and the surface of the transducer element **16** may either be flat, as in transducer **16***a* in FIG. **8**, or arcuate in shape, as shown in transducer **16***b* of FIG. **9**. The flat transducer **16***a* of FIG. **8** generates a collimated beam **17**, whereas the curvilinear transducer **16***b* of FIG. **9** has a focal point P that is behind the emitting surface to generate a diverging beam **19** (defocused or lens configuration preferably in the y-z plane) across a field of view from A to B (centered on C). The curvilinear transducer **16***b* of FIG. **9** helps get a 3-D volume while scanning, and is particularly useful with line arrays such as those in FIG. **5**, FIG. **10**, FIG. **11**, and FIG. **13**.

[0083] In one embodiment, exemplary dimensions for the arrays **14***a* and **14***b* and transducers **16** are as follows: a length inside the water tank along X-axis (the horizontal direction) of 16 inches, with 19.2 inches along Y-axis (the horizontal direction) and 16 inches in height along Z-axis (the vertical direction). The distances from the ends of the ultrasound phased transducer arrays **14***a* and **14***b* to the inside walls of

the water tank along X-axis are approximately 3.8425 inches. In one embodiment, the horizontal distance between the front surfaces of the two parallel phased ultrasound transducer arrays can be adjusted from 12 cm to 25 cm, with a 1 cm increment utilizing 14 different sets of spacer blocks. The accuracy and precision of the horizontal position is ideally 5 microns or better. The vertical travel (Z axis) of the two parallel ultrasound phased transducer arrays **14***a* and **14***b* is 10 inches from the top surface of the water level. The vertical travel step interval can be adjusted to any value, such as 0.25 mm, 0.5 mm, 1 mm, and 2 mm.

[0084] In one embodiment, array **14***a*, **14***b* parameters are as follows: center frequency of 1.5 MHz, bandwidth of ~80% bandwidth (−6 dB) (measured for two-way sound propagation energy), the open angle of ultrasound waves emitting from a single element at ~80°, with uniform transducer elements **16** (<1 dB variation, and uniform bandwidth for one-way sound propagation energy).

[0085] In one embodiment, the arrays **14***a*, **14***b* comprise 1.5 MHz arrays with 384 elements each, equally spaced along the array. In one example, the dimensions characteristics of the transducer elements are as follows: elevation aperture: 15 mm, element width: 0.4 mm for 1.5 MHz arrays, elevation focus: 10 cm away from the transducer element, with all transducers configured to be aligned along the array and perpendicular to the elevation plane.

[0086] It is appreciated that the above dimensions and configuration details are for reference purposes only, and such characteristics may be varied accordingly.

[0087] The advantage of the configuration of scanner **12**, over, e.g. the planar arrays of FIG. **6**, is that the system **10** is using a fewer number of transducer elements.

[0088] B. Dual Parallel Planar Array Scanner

[0089] FIG. **6** illustrates a scanner **100** comprising two parallel planar arrays **102***a* and **102***b* aligned opposing each other across the scanning medium **44**. Arrays **102***a* and **102***b* each comprise matching grids of 2-D arrays of transducers **16** (e.g. transducers **16** share the same locations in their respective x-z planes shown in FIG. **6**). With the planar arrays the scanner **100** generally does not need to be translated in the z (vertical) direction.

[0090] There are generally two limitations for the synthetic-aperture breast ultrasound tomography with the cylindrical or circular transducer arrays: (a) it is difficult to image the axillary region of the tissue **44**; and (b) one size of the cylindrical or circular transducer array will either be undersized or oversized for most sizes of the breast.

[0091] Synthetic-aperture breast ultrasound tomography with two parallel planar ultrasound transducer arrays **102***a* and **102***b* can overcome these two limitations. As shown in FIG. **6**, one planar/2D transducer array **102***b* can be placed close to the axillary region of the tissue **44**. In addition, the distance between the two planar ultrasound transducer arrays **102***a* and **102***b* can be adjusted with respect to each other (either manually or with robotic stage **90** as shown in FIG. **5**) to fit different sizes of the breast. The ultrasound transducer elements **16** can be in circular or rectangular shape, and the surface of the transducer element can be either flat or arc-shaped, as shown in FIG. **8** and FIG. **9**.

[0092] C. Cylindrical Array Scanner

[0093] FIG. **7** shows a cylindrical array scanner **110** having a cylindrical 2-D array **112***a* of transducers **16** in the inside surface of the cylinder wall **118** of the ultrasound transducer array. A planar array of elements **112***b* may also be positioned on the bottom surface **116** of the cylinder, which would primarily capture backscattered signals.

[0094] With the singular cylindrical array scanner **110**, a first half of the semi-cylinder elements **16** will be opposed to or facing the second half of the semi-cylinder elements **16**, and thus be positioned to receive direct transmission signals **30** (see FIG. **3**) at least at varying degrees of angles of incidence. Thus depending on the amount of defocusing within each transducer, a plurality, or all, of the non-emitting transducers **16** will be able to receive a direct transmission signal **30** (FIG. **3**) (at varying degrees) from the emitting transducer **16**, leading to a full 3D ultrasound tomography image of the breast.

[0095] The top end **114** of the cylinder is open, such that the breast tissue **44** is immersed into the cylindrical array scanner **110** with 2D ultrasound transducer elements **16** surrounding the tissue **44**. As with previous embodiments, the ultrasound transducer elements **16** can be in circular or rectangular shape, and the surface of the transducer element can be either flat or arc-shaped, as shown in FIG. **8** and FIG. **9**.

[0096] D. Torroidal (Circular) Array Scanner

[0097] FIG. **10** shows a torroidal array scanner **120** having a circular array **122** of transducers **16** aligned in a ring that is configured to encircle the breast **44**. A robotic stage **124** may be provided to allow for translation of the array **122** to and scan the breast **44** from the chest wall to the nipple region, slice by slice.

[0098] With the singular torroidal array scanner **120**, a first half of the semi-circle elements **16** will be opposed to or facing the second half of the semi-circle elements **16**, and thus be positioned to receive direct transmission signals **30** (see FIG. **3**) at least at varying degrees of angles of incidence. Thus, depending on the amount of defocusing within each transducer, a plurality, or all, of the non-emitting transducers **16** will be able to receive a direct transmission signal **30** (at varying degrees) from the emitting transducer **16**.

[0099] The circular array **122** preferably comprises defocused lens-transducer elements **16***b* as shown in FIG. **9**, enabling 3-D breast ultrasound tomography. One advantage of the torroidal configuration **120** is using a fewer number of transducer elements compared to the cylindrical transducer array **110**.

[0100] E. Dual Torroidal (Circular) Array Scanner

[0101] FIG. **11**. shows another synthetic-aperture ultrasound breast tomography scanner **130** that incorporates use of two circular transducer arrays (upper cirular array **132***a* and lower circular array **132***b*).

[0102] Image resolution depends, at least in part, on ultrasound illumination of the target medium **44**. To increase the ultrasound out-of-plane illumination angle, an acoustic diverging lens **16***b*, as shown in FIG. **9**, may be used to widen the elevation beam to the desired level (e.g. between points B and C in the upper cirular array **132***a* and D and E in the lower circular array **132***b* (conically diverging beam)). Thus, the defocused ultrasound transducer elements **16***b* transmit ultrasound waves propagating not only to the transducer elements within the same circular array, e.g. between B and C in the upper ring **132***a*, but also to the other circular transducer array, e.g. between D and E in the lower ring **132***b*. The upper transducer array **132***a* may be configured to scan the breast **44** from the chest wall position to the nipple region. At each position, the lower transducer array **132***b* may move to different vertical position in the z-axis to acquire ultrasound data. This configuration leads to improved vertical resolution

of breast ultrasound tomography images compared that obtained using one circular transducer array as shown in FIG. **10**.

[0103] In practice, the two circular ultrasound transducer arrays **132***a* and **132***b* are immersed into the water tank **76** and both encircle the breast **44**. One or both arrays **132***a* and **132***b* may be configured to translate vertically via a motorized stage **134**. For example, during an ultrasound scan, the upper cirular array **132***a* can be positioned against the chest wall, while the lower cirular array **132***b* moves upward from below the nipple region, or vice versa.

[0104] As with previous embodiments, each element of one transducer array is fired sequentially, and all elements of both transducer arrays receive ultrasound scattering data **32**. The scanner **130** acquires not only ultrasound propagating from one element to all elements within the same transducer array, but also those ultrasound waves propagating from the emitting element to all elements of the other transducer array, leading to a full 3D ultrasound tomography image of the breast.

[0105] Such a UST system **130** allows recording of volumetric ultrasound data, and the image resolution limited by slice thickness will be alleviated. In one exemplary design, the data acquisition electronics **18** allow a maximum of 768 parallel channels, so the number of transducers may be halved per array **132***a* and **132***b*. The coarser sampling in the plane of the array will be compensated by the cross illuminations

[0106] The scanner **130** of FIG. **11** can significantly improve image resolution and quality compared to those obtained from an ultrasound tomography system with one circular transducer array. A 3D ultrasound tomography system **10** of this configuration will be operator independent, which is critical for cancer screening, and will be more cost-effective than an ultrasound tomography system with a cylindrical transducer array.

[0107] F. Combination 2D Planar and 2D-Arc Array Scanner

[0108] FIG. **12** shows a scanner **140** comprising a semicircular or arcuate array **142***b* having transducers **16** in an opposing or facing orientation with planar array **142***a*, with target tissue **44** disposed between the two. The scanner **140** provides a combination of the advantages of the cylindrical transducer array **110** with those of the 2D planner array **100**. An ultrasound tomography system **10** with such combination of transducer arrays improves the range of spatial coverage for data acquisition, and the planar array **142** can still be placed near the axillary region.

[0109] G. Combination 1D Beam and Arc Array Scanner

[0110] FIG. **13** illustrates a scanner **150** that reduces the 2D arrays in FIG. **12** to 1D arrays (arcuate line array **152***b* and linear beam array **152***a*). This configuration, using a one-dimeisional, straight-phased array **152***a* and a 1D arc-shaped array, **152** reduces the number transducers **16**, and thus the number of channels required for data acquisition electronics **18**, while improving the spatial coverage of data acquisition compared to when using a two parallel phased transducer array scanner **12** in FIG. **5**.

[0111] II. Synthetic Aperture Ultrasound Tomography Methods

[0112] Referring now to FIG. **14**, a flow chart of a synthetic aperture ultrasound tomography method **200** is shown. This method is preferably used with any of the systems and scanners shown in FIG. **1** through FIG. **14**, although other scanning systems are contemplated. Ideally, the method is used in conjunction with a scanner that has one or more arrays configured so that a plurality of transducers **16** of an array, or portion of an array, oppose (at a spaced-apart distance across the target scanning medium **44**) a plurality of transducers **16** of either another portion of the array, or a separate array, so that reflection and transmission data may be acquired with each successive transducer excitation.

[0113] At step **202**, the method performs a synthetic aperture ultrasound scan of the tissue medium in accordance with the schematic illustration of scanner **12** FIG. **3**. At step **204**, reflection and transission data are simultaneously acquired, as shown in the method **50** of FIG. **4**. At step **206**, ultrasound waveform tomagraphic imaging is performed on the acquired reflection and transmission data to generate a high-resolution ultrasound reconstruction image of the target medium **44**.

[0114] As mentioned previously, a particular shortcoming of existing ultrasound omographic imaging is that they either use only transmission data, or reflection data only, for image reconstructions. In contrast, the synthetic-aperture ultrasound tomography method **200** of the present invention acquired both ultrasound transmission and reflection data at the same time, and use both ultrasound transmission and reflection data for tomographic reconstructions to greatly improve the shapes and quantitative values of mechanical properties of abnormalities.

[0115] FIGS. **15** through **18**B demonstrate that using numerical breast-phantom data from ultrasound waveform tomography using both transmission and reflection data simultaneously significantly improves the accuracy of tomographic reconstructions, compared to those obtained using only ultrasound transmission data or only ultrasound reflection data.

[0116] Numerical phantom data was generated for a synthetic-aperture ultrasound tomography system with a two parallel phased transducer array scanner **12** as shown in FIG. **5**. Each transducer array **14***a*, **15***b* is comprised of 384 evenly distributed ultrasound transducer elements, with a pitch size of 0.55 mm. The two transducer arrays were separated by 20 cm. The ultrasound source function used is a Ricker wavelet with a central frequency of 1.0 MHz.

[0117] FIG. **15** shows an image of a numerical breast phantom containing two different tumors (small, light tumor, and larger dark tumor). The background sound-speed of the phantom was 1500 ms, and those of the two tumor speeds were 1530 ms and 1550 ms, respectively. The diameters of the tumors were 2.0 mm and 7.0 mm, and approximately 1.3 wavelengths and 4.6 wavelengths. The two tumors were positioned along the longitudinal direction relative to the ultrasound transducer arrays. A high-order finite-difference time-domain wave-equation algorithm in accordance with step **206** was used to compute ultrasound transmission and reflection data.

[0118] FIG. **16**A and FIG. **16**B show imaging results (tomographic reconstruction in FIG. **16**A, and vertical profile along the center of the tumors in FIG. **16**B) obtained using only the reflection data. FIG. **17**A and FIG. **17**B show imaging results (tomographic reconstruction in FIG. **17**A, and vertical profile along the center of the tumors in FIG. **17**B) obtained using only the transmission data. FIG. **18**A and FIG. **18**B show imaging results (tomographic reconstruction in FIG. **18**A, and vertical profile along the center of the tumors in FIG. **18**B) obtained using both transmission and reflection data simultaneously in accordance with method **200**.

[0119] The waveform tomographic reconstruction using only the reflection data (FIG. **16**A and FIG. **16**B) provides mostly the edge information of the tumors, and can distinguish the two tumors.

[0120] On the other hand, the waveform tomographic reconstruction (FIG. **17**A and FIG. **17**B) using only the transmission data gives mostly low spatial-wavenumber components of the tumors, and it is almost impossible to separate the two tumors.

[0121] By contrast, the waveform tomographic reconstruction using both the transmission and reflection data simultaneously (FIG. **18**A and FIG. **18**B) takes the advantages of the above two kinds of tomographic reconstructions, and produces an image with much improved tumor edges and sound-speed reconstructions.

[0122] A. Synthetic Aperture Ultrasound Waveform Tomography with Regularization

[0123] FIG. **19** illustrates a preferred method **206** for generating the ultrasound waveform step of method **200** (FIG. **14**) using both transmission and reflection data for ultrasound waveform tomography. As shown in FIG. **19**, reflection and transmission data are input at step **210**, and ray approximation is performed at step **212** to generate an initial model. Next at step **214**, image reconstruction is performed by computing the wave acoustic wave properties of the data by calculating the mean square difference between the observed and synthetic waveforms. In particular, step **214** is performed by performing iterative waveform inversion with regularization, as will be explained in further detail below. From a more basic level, performing step **214** is achieved by solving the acoustic wave equation of Eq. 1 with the minimization model of Eq. 5.

[0124] The acoustic-wave equation in the time-domain is given by:

$$\left[\frac{1}{K(r)}\frac{\partial^2}{\partial t^2}-\nabla\cdot\left(\frac{1}{\rho(r)}\nabla\right)\right]p(r,t)=s(r,t), \qquad \text{Eq. 1}$$

where ρ(r) is the density, K(r) is the bulk modulus, s(t) is the source term, and p(r, t) is the pressure field.

[0125] The solution to Eq. 1 can be written as:

$$p=f(K,s), \qquad \text{Eq. 2}$$

where the function of f is the forward modeling operator. Numerical techniques, such as finite-difference and spectral-element methods, can be used to solve Eq. 2. Let the model parameter be:

$$m=\begin{bmatrix}K\\ s\end{bmatrix}.$$

[0126] We can rewrite Eq. 2 as:

$$p=f(m). \qquad \text{Eq. 3}$$

[0127] For the case of constant density, Eq. 1 becomes:

$$\left(\frac{1}{C^2(r)}\frac{\partial^2}{\partial t^2}-\nabla^2\right)p(r,t)=s(r,t), \qquad \text{Eq. 4}$$

where $C(r)=\sqrt{K(r)/\rho(r)}$ is the sound speed, and the model parameter is m=C(r).

[0128] The inverse problem of Eq. 3 is posed as a minimization problem such that:

$$E(m)=\min_m \{\|d-f(m)\|_2^2\}, \qquad \text{Eq. 5}$$

where $\|d-f(m)\|_2^2$ is the misfit function, d can be either ultrasound reflection data, or ultrasound transmission data, or combined ultrasound reflection and transmission data, and $\|\cdot\|_2$ stands for the L_2 norm. The minimization of Eq. 5 comprises solving for a model m that yields the minimum mean square difference between measured and synthetic waveforms.

[0129] However, because the measurements have limited coverage, solving Eq. 5 is ill-posed. Moreover, because of the nonlinearity of the function f, the solution can be trapped in the neighborhood of a local minimum of the misfit function. Therefore, a regularization technique is preferably applied to Eq. 5 to alleviate the ill-posedness of the inversion.

[0130] A general form of regularization is often written as:

$$E(m)=\min_m\{\|d-f(m)\|_2^2+\lambda R(m)\}, \qquad \text{Eq. 6}$$

where R(m) is the regularization term.

[0131] The methods of the present invention are directed to performing ultrasound waveform tomography of acquired reflection and transmission signals with use of a regularization scheme. In particular, transmission and reflection data are used for ultrasound waveform tomography with a total variation (TV) regularization scheme and modified TV regularization scheme.

[0132] Similar to the experiments conducted with respect to FIG. **15** through FIG. **18**B, testing was also done to determine the advantage of using both transmission and reflection data for ultrasound waveform tomography with a regularization scheme. Ultrasound waveform tomography with a modified total-variation regularization scheme (discussed in further detail below) to the same numerical phantom data. FIG. **20**A through FIG. **20**B, FIG. **21**A through FIG. **21**B, and FIG. **22**A through FIG. **22**B, respectively, show tomographic reconstruction results obtained using only reflection data, only transmission data, and both transmission and reflection data. Ultrasound waveform tomography with the modified total-variation regularization significantly reduces the image artifacts, and improves the accuracy of sound-speed reconstructions. However, the tomographic reconstruction in FIG. **20**A through FIG. **20**B, obtained using only the reflection data, still gives mostly the edge information for the larger tumor. The tomographic reconstruction in FIG. **21**A through FIG. **21**B, produced using only the transmission data, cannot separate the two tumors. When using both the transmission and reflection data simultaneously, our ultrasound waveform tomography with the modified total-variation regularization gives accurate reconstructions of the shapes and the sound-speeds of both tumors.

[0133] For each of the TV regularization and modified TV regularization ultrasound waveform tomography methods of the present invention, the following description will give an overview on the derivation of the equations used to solve the particular image reconstruction, followed by a discussion of algorithms and computations methods of the present inven-

tion for generating the reconstructed images. Then, numerical results for tests showing the efficacy of both methods will be described and illustrated.

[0134] B. Synthetic Aperture Ultrasound Waveform Tomography with TV Regularization.

[0135] The Tikhonov regularization can be formulated as

$$E(m) = \min_m \{\|d - f(m)\|_2^2 + \lambda\|Hm\|_2^2\}, \quad \text{Eq. 7}$$

where the matrix H is usually defined as a high-pass filtering operator, or an identity matrix. The Tikhonov regularization is a L_2-norm-based regularization; therefore, it is best suited for the smooth parameter m. In other words, the Tikhonov regularization is not the best option for sound-speed reconstructions of small breast tumors.

[0136] The TV regularization can be written as:

$$E(m) = \min_m \{\|d - f(m)\|_2^2 + \lambda\|m\|_{TV}\}, \quad \text{Eq. 8}$$

where the TV regularization for 2D model is defined as the L_1 norm:

$$\|m\|_{TV} = \|\nabla m\|_1 = \sum_{1\le i,j\le n} \sqrt{|(\nabla_x m)_{i,j}|^2 + |(\nabla_z m)_{i,j}|^2}, \quad \text{Eq. 9}$$

with

$$(\nabla_x m)_{i,j} = m_{i+1,j} - m_{i,j}$$

and

$$(\nabla_z m)_{i,j} = m_{i,j+1} - m_{i,j}.$$

[0137] For sound-speed reconstructions of small breast tumors, the methods of the present invention exploit the TV regularization for performing ultrasound waveform tomography using both transmission and reflection data. Because of the nonlinearity of the TV term in Eq. 9 and its non-differentiability at the origin, the method of the present invention is also directed to approximate the original TV functional so that it can be differentiated. A preferred approach is to approximate the TV term as:

$$\|m\|_{TV,\epsilon} = \sum_{1\le i,j\le n} \sqrt{|(\nabla_x m)_{i,j}|^2 + |(\nabla_z m)_{i,j}|^2 + \epsilon}, \quad \text{Eq. 10}$$

where ϵ is a small positive constant, making $\|m\|_{TV,\epsilon}$ differentiable, so the gradient and Hessian can be calculated.

[0138] The role of the positive constant ϵ is to approximate the Euclidean norm |x| with a smooth function $\sqrt{|x^2|+\epsilon}$. The larger the value of ϵ, the smoother the approximation. Whereas the smaller the value of ϵ, the closer the approximation to the original function, and the more singular the approximation becomes at the origin. Therefore, we need to use a reasonable value for ϵ, which strikes a balance between a good approximation and the stability. The value of ϵ was set to be 0.1 in the numerical tests detailed below.

[0139] The other parameter used in the TV regularization function (Eq. 10) of the present invention is λ, which is configured to balance between the data fidelity term $\|d-f(m)\|_2^2$ and the regularization term $\|m\|_{TV}$. Previous methods to automatically pick the parameter have been for linear applications. Because of the nonlinearity of the problem, those methods cannot be directly applied to the TV regularization function (Eq. 10) of the present invention.

[0140] Accordingly, one method of the present invention is to pick λ, as a function of Eq. 11:

$$\lambda = \frac{\|d - f(m)\|_2^2}{r \cdot \|m\|_{TV}}, \quad \text{Eq. 11}$$

where the value of r is defined to be the ratio between the data fidelity term and the regularization term. A value of $1\times10^7<r<1\times10^8$ r was found to return reasonable results.

[0141] There are two major computational methods involved in solving for the minimization problem of Eq. 5: the forward modeling algorithm and the inverse optimization algorithm. Because the model parameters for the model m that we are solving have high dimensionality, an iterative optimization method based on the Krylov subspace is used, or Nonlinear Conjugate Gradient (NCG).

[0142] One critical step in the optimization is the calculation of the measurements for given model parameters, which is usually called forward modeling. It is usually the most computationally intensive. Here, for the forward modeling, the finite-difference method with staggered grids in both space and time domain was used.

[0143] Instead of using the wave equation, which is a second-order hyperbolic equation, we use the equivalent first-order equations for illustration:

$$\begin{cases} \dfrac{\partial p}{\partial t} + K(r)\left(\dfrac{\partial u}{\partial x} + \dfrac{\partial v}{\partial z}\right) = s(r,t), \\ \dfrac{\partial u}{\partial t} + \dfrac{1}{\rho(r)}\dfrac{\partial p}{\partial x} = 0, \\ \dfrac{\partial v}{\partial t} + \dfrac{1}{\rho(r)}\dfrac{\partial p}{\partial z} = 0, \end{cases} \quad \text{Eq. 12}$$

where u is the wavefield velocity along the x direction, and v is the wavefield velocity along the z direction. If a two-point central finite-difference scheme is used to approximate the derivative in the time domain, and a fourth-order Taylor expansion is used to interpolate for the derivative values in the space domain, this finite-difference scheme yields a fourth-order accuracy in space and a second-order accuracy in time. The superscripts and subscripts are meant to distinguish between increments in time and space:

$$\begin{cases} p_{i,j+1/2}^{k+1/2} = p_{i,j+1/2}^{k-1/2} + K_{i,j+1/2}\dfrac{\delta t}{\delta x}\left[\left(\dfrac{\partial u}{\partial x}\right)_{i,j+1/2}^{k-1/2} + \left(\dfrac{\partial v}{\partial z}\right)_{i,j+1/2}^{k-1/2}\right] + s(r,t), \\ u_{i+1/2,j+1/2}^{k+1/2} = u_{i+1/2,j+1/2}^{k-1/2} + \dfrac{1}{\rho_{i+1/2,j+1/2}}\left(\dfrac{\partial p}{\partial x}\right)_{i+1/2,j+1/2}^{k-1/2}, \\ v_{i,j}^{k+1/2} = v_{i,j}^{k-1/2} + \dfrac{1}{\rho_{i,j}}\left(\dfrac{\partial p}{\partial z}\right)_{i,j}^{k-1/2}, \end{cases} \quad \text{Eq. 13}$$

where

-continued

$$\begin{cases} \left(\frac{\partial u}{\partial x}\right)_{i,j+1/2} = 0.0417\left(u_{i-3/2,j+1/2} - u_{i+3/2,j+1/2}\right) + 1.125\left(u_{i-1/2,j+1/2} - u_{i+1/2,j+1/2}\right), \\ \left(\frac{\partial v}{\partial z}\right)_{i,j+1/2} = 0.0417(v_{i,j-1} - v_{i,j+2}) + 1.125(v_{i,j} - v_{i,j+1}), \\ \left(\frac{\partial p}{\partial x}\right)_{i+1/2,j+1/2} = 0.0417\left(p_{i-1,j+1/2} - p_{i+2,j+1/2}\right) + 1.125\left(p_{i,j+1/2} - p_{i+1,j+1/2}\right), \\ \left(\frac{\partial p}{\partial z}\right)_{i,j} = 0.0417\left(p_{i,j-3/2} - p_{i,j+3/2}\right) + 1.125\left(p_{i,j-1/2} - p_{i,j+1/2}\right). \end{cases} \quad \text{Eq. 14}$$

[0144] NCG was used to solve the optimization problem in Eq. 8. The gradient of the cost function is needed for computing the search direction. The gradient of the cost function E(m) is needed for computing the search direction. The gradient of the data misfit can be obtained using the adjoint-state method:

$$\nabla_m \|d - f(m)\|_2^2 = 2\rho(C^{(k)}(r))^2 \sum_{shots} \sum_{t} \nabla \cdot \vec{u}^{(k)}(r,t) \nabla \cdot \overleftarrow{b}^{(k)}(r,t), \quad \text{Eq. 15}$$

where $\vec{u}^{(k)}$ is the forward propagated wavefield, and $\overleftarrow{b}^{(k)}$ is the backward propagated residual at iteration k, which is defined as $r^{(k)}=d^{obs}-f(m^{(k)})$

[0145] The gradient of the TV term is obtained using:

$$\nabla_m TV(m) = [D_x^T \; D_z^T] \begin{bmatrix} \mathrm{diag}(\phi'(m)) & 0 \\ 0 & \mathrm{diag}(\phi'(m)) \end{bmatrix} \begin{bmatrix} D_x \\ D_z \end{bmatrix} m, \quad \text{Eq. 16}$$

where $\phi(t)=\sqrt{t^2+\epsilon}$, $\phi'(m)=\phi'(D_x m^2+D_z m^2)$ and the spatial derivative $D_x m=m_{i+1,j}-m_{i,j}$ and $D_z m=m_{i,j+1}-m_{i,j}$ for the spatial grid indices i and j.

[0146] Therefore, the gradient of the cost function E(m) is:

$$\nabla_m E(m)=\nabla_m \|d-f(m)\|_2^2+\nabla_m TV(m). \quad \text{Eq. 17}$$

[0147] The search direction $q_{(k)}$ at iteration k is then defined to be the conjugate to the gradient at the current iteration step. Once the search direction $q^{(k)}$ at iteration k is obtained, the line search with the following Armijo criteria is further used for the optimal step size $\beta^{(k)}$:

$$\begin{cases} E(m^{(k)} + \beta^{(k)} q^{(k)}) & \le E(m^{(k)}) + c_1 \beta^{(k)} (q^{(k)})^T \nabla E(m^{(k)}), \\ (q^{(k)})^T \nabla E(m^{(k)} + \beta^{(k)} q^{(k)}) & \ge c_2 (q^{(k)})^T \nabla E(m^{(k)}). \end{cases} \quad \text{Eq. 18}$$

[0148] When the search direction $q^{(k)}$ and the step size $\beta^{(k)}$ are determined, the update of the current iteration is updated according to Eq. 19:

$$m^{(k+1)}=m^{(k)}+\beta^{(k)} q^{(k)} \quad \text{Eq. 19}$$

[0149] FIG. **23** illustrates a flow diagram for a method **220** for performing the computing step **214** of FIG. **19**. This is achieved via solving the acoustic wave (Eq. 1) by using the NCG based algorithm (Algorithm 1 below) to approximate the TV regularization term (Eq. 8) according to Eq. 10.

[0150] Referring to FIG. **23**, the first step in the method **220** is to input the specified tolerance TOL, in addition to the initial model $m^{(0)}$. Other parameters, such as λ, which is preferably determined according to the method of the present invention shown in Eq. 11, may also be input in this step. The initial model $m^{(0)}$ may be generated via applying the ray approximation step **212** of the input reflection and transmission data **210**, as shown in FIG. **19**.

[0151] At step **224**, the parameters are initialized (e.g. the current iteration value k is set at zero).

[0152] At step **226**, the algorithm queries whether the current iteration of the model has met the minimum value set by the assigned tolerance TOL.

[0153] If the threshold value has not been met, the algorithm computes the step size by computing Eq. 18 at step **228**.

[0154] Next, at step **230**, the current iteration model $m^{(k)}$ is updated based on step size $\beta^{(k)}$ and search direction $q^{(k)}$ according to Eq. 19.

[0155] At step **332**, the gradient of the cost function $\nabla E^{(k+1)}$ is computed according to Eq. 17.

[0156] At step **234**, the ratio of the inner product of the gradient VE is computed to find the term $\gamma^{(k+1)}$ according to:

$$\gamma^{(k+1)} = \frac{<\nabla E^{(k+1)}, \nabla E^{(k+1)}>}{<\nabla E^{(k)}, \nabla E^{(k)}>}.$$

[0157] Finally, the search direction $q^{(k)}$ is updated at step **236** according to:

$$q^{(k+1)}=-\nabla E^{(k+1)}+\gamma^{(k+1)} q^{(k)}$$

[0158] The current iteration value k is then updated and the process repeated at step **238**.

[0159] If the threshold tolerance has been met at step **226**, then the process ends and outputs the model $m^{(k)}$ at step **240**. If not, the process continues to iterate until it does.

Algorithm 1: Canonical NCG to solve $\min_m$ E(m) in Eq. 8

Input: $m^{(0)}$, TOL
Output: $m^{(k)}$
1: Initialize k = 0, $E^{(0)} = E(m^{(0)})$, $\nabla E^{(0)} = \nabla E(m^{(0)})$, and $q^{(0)} = \nabla E^{(0)}$;
2: while $\{||\nabla E^{(k)}|| > TOL\}$ do
3: Compute the step size $\beta^{(k)}$ satisfying Eq. 18;
4: Update the solution according to Eq. 19;
5: Compute the gradient $\nabla E^{(k+1)}$ based on Eq. 17;
6: Compute the ratio of the inner product of the gradient VE :

$$\gamma^{(k+1)} = \frac{\langle \nabla E^{(k+1)}, \nabla E^{(k+1)} \rangle}{\langle \nabla E^{(k)}, \nabla E^{(k)} \rangle};$$

7: Update the search direction: $q^{(k+1)} = -\nabla E^{(k+1)} + \gamma^{(k+1)} q^{(k)}$;
8: Next iteration: k ← k + 1;
9: end while

[0160] C. Synthetic Aperture Ultrasound Waveform Tomography with Modified TV Regularization.

[0161] The conventional TV regularization discussed above suffers from slow convergence. Thus, a modified TV regularization scheme may to be adapted into ultrasound waveform tomography.

[0162] The cost function with the modified TV regularization is given by:

$$E(m,u)=\min_{m,u}\{\|d-f(m)\|_2^2+\lambda_1\|m-u\|_2^2+\lambda_2\|\nabla u\|_1\},\qquad \text{Eq. 20}$$

where λ_1 and λ_2 are both positive regularization parameters, and an auxiliary variable u is added to the conventional TV functional in Eq. 8.

[0163] Hence, the modified TV regularization in Eq. 20 can be equivalently written as

$$E(m,u)=\min_u\left\{\min_m\{\|d-f(m)\|_2^2+\lambda_1\|m-u\|_2^2\}+\lambda_2\|\nabla u\|_1\right\},\qquad \text{Eq. 21}$$

[0164] An alternating-minimization algorithm can therefore be employed for solving the double minimization problem in Eq. 21. Beginning with a starting model $u^{(0)}$, solving for Eq. 21 leads to the solutions of two minimization problems:

$$\begin{cases} m^{(k)}=\underset{m}{\operatorname{argmin}}\|d-f(m)\|_2^2+\lambda_1\|m-u^{(k-1)}\|_2^2 \\ u^{(k)}=\underset{u}{\operatorname{argmin}}\|m^{(k)}-u\|_2^2+\lambda_2\|\nabla u\|_1 \end{cases}\qquad \text{Eq. 22}$$

for i=1, 2, ... We describe the computational methods for solving these two minimization problems in Eq. 22. Compared to the conventional TV function in Eq. 8, the benefits of solving the modified TV functional by adding the auxiliary variable u in Eq. 22 are twofold. First, we simplify the complexity of the original optimization problem of nonlinear inversion with the TV constraint. From Eq. 22, these two sub-optimization problems have distinct physical meanings: solving for $m^{(k)}$ is the nonlinear inversion with a Tikhonov regularization constraint; solving for $u^{(k)}$ is to preserve the edges. Therefore, the interleaving of solving these two variables leads to a solution minimizing the data misfit term with edges preserved. The other benefit that we gain out of solving Eq. 22 is that solving for $u^{(k)}$ is a typical L_1-TV problem, and we can smartly choose certain computational methods, such that the selection of the smoothing parameter of ϵ in Eq. 10 can be avoided.

[0165] Selecting the right values for the parameters used in the conventional and modified TV regularization schemes is important for the effective use of these regularization schemes.

[0166] The role of the positive constant E is to approximate the Euclidean norm $\|x\|$ with a smooth function $\sqrt{\|x^2\|+\epsilon}$ as in Eq. 10. The larger the value of ϵ, the smoother the approximation, whereas the smaller the value of ϵ, the closer the approximation to the original function, and the more singular the approximation becomes at the origin. Therefore, we need to use a reasonable value for ϵ, which strikes a balance between a good approximation and stability. Otherwise, an inappropriate selection of ϵ not only can result in inaccurate results, but also can significantly increase the number of iterations required. The following method of the present invention the is used to solve the optimization problem and allows us to avoid the selection of this smoothing parameter ϵ.

[0167] The other parameters used in Eq. 22 are λ_1 and λ_2. From the above formulation, the meaning of two regularization parameters can be specifically determined. The parameter λ_1 controls the trade-off between the data misfit term $\|d-f(m)\|_2^2$ and the regularization term $\|m-u^{(k-1)}\|_2^2$, and λ_2 controls the amount of edge-preservation to the reconstruction. Existing methods all rely on an explicitly constructed forward operator A, such that the trace value of $A(A^T+\lambda I)^{-1}A^T$ is required to proceed the estimation of the regularization parameters.

[0168] In the method of the present invention, λ_1 and λ_2 are selected such that:

$$\lambda_i=\frac{\text{data fidelity term}}{r_i\cdot\text{regularization term}},\ i=1,2,\qquad \text{Eq. 23}$$

where the values of r_i are defined to be the ratio between the data fidelity term and the regularization term. We find that $1\times10^7<r_1<1\times10^8$, and $0.1<r_2<1$ usually yield reasonably good reconstruction results.

[0169] Solving for the minimization problem in Eq. 20 is decomposed into solving two separate minimization problems:

$$E(m)=\min_m\|d-f(m)\|_2^2+\lambda_1\|m-u^{(k-1)}\|_2^2,\qquad \text{Eq. 24}$$

and

$$E(u)=\min_u\|u-m^{(k)}\|_2^2+\lambda_2\|u\|_{TV}.\qquad \text{Eq. 25}$$

[0170] Therefore, a sequence of iterations are generated, specifically

$$u^{(0)},m^{(1)},u^{(1)},m^{(2)},u^{(2)},m^{(3)},u^{(3)},\ldots,m^{(k)},u^{(k)},\ldots.$$

which is shown in more detail in the computational method **250** of FIG. **24** for solving Eq. 20, and is embodied in Algorithm 2 below.

[0171] In the following, the computational methods for solving Eq. 20 and the two minimization problems of Eq. 24 and Eq. 25 in accordance with the present invention are shown with reference to FIG. **24**, FIG. **25**, and FIG. **26**, in addition to Algorithms 2, 3, and 4 below.

[0172] Referring to FIG. **24**, the computational method **250** for solving Eq. 20 comprises first inputting the specified tolerance TOL, in addition to the initial model $u^{(0)}$ at step **252**. Other parameters, such as λ, which is preferably determined according to the method shown in Eq. 23 of the present invention, may also be input in this step. The initial model $u^{(0)}$ may be generated via applying ray approximation step **212** on the input reflection and transmission data **210** as shown in FIG. **19**.

[0173] At step **254**, the parameters are initialized (e.g. the current iteration value k is set at zero).

[0174] A step **256**, the algorithm queries whether the current iteration of the model has met the minimum value set by the assigned tolerance TOL.

[0175] If the threshold value has not been met, the algorithm solves Eq. 24 to compute $m^{(k)}$ according to Algorithm 3 and method **270** of FIG. **5** at step **258**.

[0176] At step **260**, $u^{(k)}$ is computed according to Algorithm 4 and method **300** of FIG. **26**. The current iteration value is then updated at step **262**, and the routine returns to step **256**. If the threshold is met, the algorithm ends and outputs $u^{(k)}$ at step **264**. If not, Algorithm 2 continues to iterate.

Algorithm 2 Computational method for solving Eq. 20

Input: $u^{(0)}$, TOL
Output: $u^{(k)}$
1: Initialize k = 0 ;
2: while { $\| m^{(k)} - m^{(k-1)} \| >$ TOL } do
3: Solve Eq. 24 for $m^{(k)}$ according to Alg. 3;
4: Solve Eq. 25 for $u^{(k)}$ according to Alg. 4;
5: Next iteration: k ← k + 1 ;
6: end while

[0177] The minimization problem of Eq. 24 (step **258** of FIG. **24**) is a conventional Tikhonov-type nonlinear-regularization problem. Accordingly, a NCG is used as the optimization method. To use NCG for solving Eq. 24, the gradient of the cost function is required to compute the search direction. The gradient of the data misfit can be obtained by the adjoint-state method:

$$\nabla_m \|d - f(m)\|_2^2 = 2\rho(C^{(k)}(r))^2 \sum_{shots} \sum_{t} \nabla \cdot \vec{u}^{(k)}(r,t) \nabla \cdot \overleftarrow{b}^{(k)}(r,t), \quad \text{Eq. 26}$$

where $\vec{u}^{(k)}$ is the forward propagated wavefield, and $\overleftarrow{b}^{(k)}$ is the backward propagated residual at iteration k, which is further defined as $r^{(k)}=d^{obs}-f(m^{(k)})$.

[0178] Therefore, the gradient of the cost function E(m) is:

$$\nabla_m E(m) = 2\rho(C^{(k)}(r))^2 \sum_{shots} \sum_{t} \nabla \cdot \vec{u}^{(k)}(r,t) \nabla \cdot \overleftarrow{b}^{(k)}(r,t) + 2\lambda_1 (m - u^{(i-1)}). \quad \text{Eq. 27}$$

[0179] The search direction $q^{(k)}$ at iteration k is then defined to be the conjugate to the gradient at the current iteration step. Once the search direction $q^{(k)}$ at iteration k is obtained, the line search with the Armijo criteria below is further used for the optimal step size $\beta^{(k)}$:

$$\begin{cases} E(m^{(k)} + \beta^{(k)} q^{(k)}) & \le E(m^{(k)}) + c_1 \beta^{(k)} (q^{(k)})^T \nabla E(m^{(k)}) \\ (q^{(k)})^T \nabla E(m^{(k)} + \beta^{(k)} q^{(k)}) & \ge c_2 (q^{(k)})^T \nabla E(m^{(k)}). \end{cases} \quad \text{Eq. 28}$$

[0180] With the search direction $q^{(k)}$ and the step size $\beta^{(k)}$ determined, the update of the current iteration is therefore given by:

$$m^{(k+1)} = m^{(k)} + \beta^{(k)} q^{(k)} \quad \text{Eq. 29}$$

[0181] The NCG algorithm **270** shown in FIG. **25**, used for solving Eq. 24, is also in Algorithm 3. The first step in the method **270** is to input the specified tolerance TOL, in addition to the initial model $m^{(0)}$. Other parameters, such as λ_1 and λ_2, which are preferably determined according to the method of the present invention shown in Eq. 23, may also be input in this step. The initial model $m^{(0)}$ may be generated via applying ray approximation step **212** of the input reflection and transmission data **210** as shown in FIG. **19**.

[0182] At step **274**, the parameters are initialized (e.g. the current iteration value k is set at zero).

[0183] A step **276**, the algorithm queries whether the current iteration of the model has met the minimum value set by the assigned tolerance TOL.

[0184] If the threshold value has not been met, the algorithm computes the step size by computing Eq. 28 at step **278**.

[0185] Next, at step **280**, the current iteration model $m^{(k)}$ is updated based on step size $\beta^{(k)}$ and search direction $q^{(k)}$ according to Eq. 29.

[0186] At step **282**, the gradient of the cost function $\nabla E^{(k+1)}$ is computed according to Eq. 27.

[0187] At step **284**, the ratio of the inner product of the gradient VE is computed to find the term $\gamma^{(k+1)}$ according to:

$$\gamma^{(k+1)} = \frac{< \nabla E^{(k+1)}, \nabla E^{(k+1)} >}{< \nabla E^{(k)}, \nabla E^{(k)} >}.$$

[0188] Finally, the search direction $q^{(k)}$ is updated at step **286** according to:

$$q^{(k+1)} = -\nabla E^{(k+1)} + \gamma^{(k+1)} q^{(k)}$$

[0189] The current iteration value k is then updated at step **288**, and the process repeated at step **276**.

[0190] If the threshold tolerance has been met at step **276**, then the process ends, and outputs the model $m^{(k)}$ at step **290**. If not, the process continues to iterate until it does.

Algorithm 3: Canonical NCG to solve $\min_m E(m)$

Input: $m^{(0)}$, TOL
Output: $m^{(k)}$
1: Initialize k = 0, $E^{(0)} = E(m^{(0)})$, $\nabla E^{(0)} = \nabla E(m^{(0)})$, and $q^{(0)} = \nabla E^{(0)}$;
2: while $\{||\nabla E^{(k)}|| > \text{TOL}\}$ do
3: Compute the step size $\beta^{(k)}$ satisfying Eq. (28);
4: Update the solution according to Eq. (29);
5: Compute the gradient $\nabla E^{(k+1)}$ based on Eq. (27);
6: Compute the ratio of the inner product of the gradient ∇E :

$$\gamma^{(k+1)} = \frac{\langle \nabla E^{(k+1)}, \nabla E^{(k+1)} \rangle}{\langle \nabla E^{(k)}, \nabla E^{(k)} \rangle};$$

7: Update the search direction: $q^{(k+1)} = -\nabla E^{(k+1)} + \gamma^{(k+1)} q^{(k)}$;
8: Next iteration: k ← k + 1;
9: end while

[0191] While there are many numerical methods for solving the L_2-TV problem describing in Eq. 25, the split-Bregman method approach was found to be appropriate. Optimization problems of the L_1-TV or L_2-TV type are most efficiently solved by using the Bregman distance, which is defined as

$$D_E^p(u,v) = E(u) - E(v) - \langle p, u - v \rangle, \quad \text{Eq. 30}$$

where p is the subgradient of E at v. The basic idea of the split-Bregman method is to reformulate Eq. 25 as an equivalent minimization problem based on the Bregman distance:

$$E(u, g_x, g_z) = \min_{u,g_x,g_z} \|u - m^{(k)}\|_2^2 + \lambda_2\|u\|_{TV} + \mu\|g_x - \nabla_x u - b_x^{(k)}\|_2^2 + \mu\|g_z - \nabla_z u - b_z^{(k)}\|_2^2, \quad \text{Eq. 31}$$

where

$$g_x^{(k)} = \nabla_x u^{(k)},\ g_z^{(k)} = \nabla_z u^{(k)},\ b_x^{(k+1)} = b_x^{(k)} + (\nabla_x u^{(k+1)} - g_x^{(k+1)}),$$

and

$$b_z^{(k+1)} = b_z^{(k)} + (\nabla_z u^{(k+1)} - g_z^{(k+1)}).$$

[0192] To solve this minimization problem, an alternating minimization algorithm is employed to Eq. 31, where two subproblems need to be further minimized:

$$E(u) = \min_u \|u - m^{(k)}\|_2^2 + \mu\|g_x^{(k)} - \nabla_x u - b_x^{(k)}\|_2^2 + \mu\|g_z^{(k)} - \nabla_z u - b_z^{(k)}\|_2^2, \quad \text{Eq. 32}$$

and

$$E(g_x, g_z) = \min_{g_x,g_z} \lambda_2\|u\|_{TV} + \mu\|g_x - \nabla_x u - b_x^{(k)}\|_2^2 + \mu\|g_z - \nabla_z u - b_z^{(k)}\|_2^2. \quad \text{Eq. 33}$$

[0193] Eq. 32 satisfies the optimality condition:

$$(I - \mu\Delta)u^{(k+1)} = m^{(k)} + \mu\nabla_x{}^T(g_x^{(k)} - b_x^{(k)}) + \mu\nabla_z{}^T(g_z^{(k)} - b_z^{(k)}) \quad \text{Eq. 34}$$

[0194] The solution of this equation is obtained using the Gauss-Seidel iterative method:

$$u_{i,j}^{(k)} = \frac{\mu}{1+4\mu}\left(u_{i+1,j}^{(k)} + u_{i-1,j}^{(k)} + u_{i,j+1}^{(k)} + u_{i,j-1}^{(k)} + g_{x,i-1,j}^{(k)} - g_{x,i,j}^{(k)} + g_{z,i,j-1}^{(k)} - g_{z,i,j}^{(k)} - b_{x,i-1,j}^{(k)} + b_{x,i,j}^{(k)} - b_{z,i,j-1}^{(k)} + b_{y,i,j}^{(k)}\right) + \frac{1}{1+4\mu} m_{i,j}^{(k)}. \quad \text{Eq. 35}$$

[0195] Equation 33 is solved explicitly using a generalized shrinkage formula:

$$g_x^{(k+1)} = \max(s^{(k)} - \lambda_2/2\mu, 0)\frac{\nabla_x u^{(k)} + b_x^{(k)}}{s^{(k)}}, \quad \text{Eq. 36}$$

and

$$g_z^{(k+1)} = \max(s^{(k)} - \lambda_2/2\mu, 0)\frac{\nabla_z u^{(k)} + b_z^{(k)}}{s^{(k)}}, \quad \text{Eq. 37}$$

where

$$s^{(k)} = \sqrt{|\nabla_x u^{(k)} + b_x^{(k)}|^2 + |\nabla_z u^{(k)} + b_z^{(k)}|^2}.$$

[0196] The numerical algorithm **300** of FIG. **26** for solving Eq. 31 using the split-Bregman iteration scheme is also provided in Algorithm 4.

[0197] The first step in the method **300** is to input the specified tolerance TOL, in addition to the initial model in addition to the initial model $u^{(0)}$ at step **302**. The initial model $u^{(0)}$ may be generated via applying ray approximation step **212** on the input reflection and transmission data **210** as shown in FIG. **19**.

[0198] At step **304**, the parameters are initialized (e.g. the current iteration value k is set at zero).

[0199] At step **306**, the algorithm queries whether the current iteration of the model has met the minimum value set by the assigned tolerance TOL.

[0200] If the threshold value has not been met, the algorithm solves Eq. 32 using the Gauss-Seidel equation (Eq. 35) at step **308**.

[0201] At step **310**, Eq. 32 is then solved using generalized shrinkage (Eq. 36 and Eq. 37).

[0202] Next, the intermediate variable b_x is updated according to $b_x^{(k+1)} = b_x^{(k)} + (\nabla_x u^{(k+1)} - g_x^{(k+1)})$ at step **312**.

[0203] The intermediate variable b_z is then updated according to $b_x^{(k+1)} = b_x^{(k)} + (\nabla_z u^{(k+1)} - g_x^{(k+1)})$ at step **314**.

[0204] The current iteration value is then updated at step **316**, and the routine returns to step **306**. If the threshold is met, the algorithm ends and outputs $u^{(k)}$ at step **318**. If not, Algorithm 4 continues to iterate.

Algorithm 4: Split-Bregman iteration

Input: $u^{(0)}$, TOL
Output: $u^{(k)}$
1: Initialize k = 0, $g_x^{(0)} = g_z^{(0)} = b_x^{(0)} = b_z^{(0)} = 0$;
2: while $\{ \| u^{(k)} - u^{(k-1)} \| > \text{TOL} \}$ do
3: Solve Eq. (32) according to Eq. (35);
4: Solve Eq. (33) according to Eq. (36) and Eq. (37);
5: Update $b_x^{(k+1)} = b_x^{(k)} + (\nabla_x u^{(k+1)} - g_x^{(k+1)})$;
6: Update $b_z^{(k+1)} = b_z^{(k)} + (\nabla_z u^{(k+1)} - g_z^{(k+1)})$;
7: Next iteration: k ← k + 1;
8: end while

[0205] To better understand the computational methods in Algorithm 2, it is worthwhile to calculate the computational costs of each of its steps.

[0206] Let the size of the model be $m \in \Re^{\tilde{m}\times\tilde{n}}$ and the data $p \in \Re^{\tilde{q}\times\tilde{n}}$ where $\tilde{m}$ is the depth, $\tilde{n}$ is the offset, and $\tilde{q}$ is the time steps. Assuming that there are s sources and the finite-difference calculation employs a scheme of $o(\delta t^2, \delta h^4)$. The total cost of Alg. 2 for one iteration step is the sum of the cost from Alg. 3 and the cost from Alg. 4. By adding the costs from all the steps in Alg. 3, the approximated cost for each iteration step is:

$$\text{COST}_1 \approx (l+3)\cdot O(s\cdot\tilde{m}\cdot\tilde{n}\cdot\tilde{q}) + (l+5)\cdot O(\tilde{m}\cdot\tilde{n}), \quad \text{Eq. 38}$$

where l is the number of trials in step **278** in the search for $\beta^{(k)}$. By assuming that Alg. 3 converges within k_1 iterations, we further approximate the cost in Eq. 38 as,

$$\text{COST}_1 \approx k_1\cdot(l+3)\cdot O(s\cdot\tilde{m}\cdot\tilde{n}\cdot\tilde{q}) + (l+5)\cdot O(\tilde{m}\cdot\tilde{n}). \quad \text{Eq. 39}$$

[0207] The most expensive part stems from the first term in Eq. 39, which is dominated by step **278** and step **282** in method **270**, and the number of iterations in Alg. 3. The cost of Alg. 4 is more straightforward. It includes the cost from the Gauss-Seidel iteration in Eq. 35 (step **308**), and the shrinkage formula in Eqs. 36 and 37 (step **310**). Hence we have Eq. 40:

$$\text{COST}_2 \approx 18\cdot O(\tilde{m}\cdot\tilde{n}). \quad \text{Eq. 40}$$

[0208] The total computational cost of Alg. 2 becomes,

$$\text{COST} \approx k_2\cdot[k_1\cdot(l+3)\cdot O(s\cdot\tilde{m}\cdot\tilde{n}\cdot\tilde{q}) + (l+23)\cdot O(\tilde{m}\cdot\tilde{n})], \quad \text{Eq. 41}$$

where k_2 is the total number of iterations in Alg. 3. We see from Eq. 41 that the extra cost of solving Eq. 25 is trivial compared to the cost of solving Eq. 24.

[0209] Two groups of tests were performed to illustrate the feasibility and efficiency of the ultrasound waveform tomography method with modified total-variation regularization in accordance with the present invention. Ultrasound waveform tomography reconstructions were first provided using the Tikhonov regularization and the conventional TV regularization for comparison. Results for numerical breast phantoms

with tumors of different diameters are shown to further illustrate the improved resolution of the ultrasound waveform tomography method of the present invention compared to that of the other methods.

[0210] We used synthetic-aperture ultrasound data from two parallel transducer arrays to test the capability of ultrasound waveform tomography with the modified TV regularization scheme of the present invention for reconstructing the sound speed of small breast tumors. We also compare the result with that obtained using the Tikhonov regularization and the conventional TV regularization. The geometry of synthetic-aperture ultrasound tomography system with two parallel transducer arrays is schematically illustrated in FIG. **5**. Each transducer array **14***a* and **14***b* comprises of 384 transducer elements **16** evenly distributed, with a pitch size of 0.55 mm. The two transducer arrays **14***a* and **14***b* are separated by 20 cm. The ultrasound source function used is a Ricker wavelet with a central frequency of 1.0 MHz.

[0211] A numerical breast phantom as shown in FIG. **27**A to test the ultrasound waveform tomography methods. The background sound speed is 1500 m/s. The sound speeds of the two small tumors are 1545 m/s and 1560 ms and their diameters are 2.2 mm and 3.0 mm, respectively. These diameters represent approximately 1.5 wavelengths and 2.0 wavelengths.

[0212] We conducted ultrasound waveform tomography with the Tikhonov regularization using simulated ultrasound transmission and reflection data, and produce the reconstruction image in FIG. **28**A. Both tumors are reasonably well reconstructed. However, the reconstructed sound-speed value of the smaller tumor is smaller than its true value. Moreover, the interfaces of the two objects are smoothed to some extent.

[0213] We applied ultrasound waveform tomography with the conventional TV regularization scheme to the same synthetic-aperture ultrasound data, and produced the reconstruction image in FIG. **28**B. The blurring effect of the Tikhonov reconstruction has been mostly eliminated. The edges of the two small breast tumors are very well preserved. However, we also notice that there are some "ringing" artifacts generated in the inner regions of the tumors.

[0214] We then employed the ultrasound waveform tomography with the modified TV regularization to the same data, and show the reconstruction result in FIG. **28**C. By comparing to FIG. **28**A and FIG. **28**B, we see that not only the edges have been very well preserved, but also the "ringing" artifacts have been mostly eliminated.

[0215] To better visualize the quantitative sound-speed values, we plotted the horizontal profiles for FIG. **28**A through FIG. **28**C at two different locations: one at the vertical position of 103 mm as shown in FIG. **30**A through FIG. **30**C, and the other at the vertical position of 98 mm as displayed in FIG. **29**A through FIG. **29**C. For the smaller breast tumor, the waveform tomography reconstruction using the Tikhonov regularization gives the sound speed value of 1540 m/s, while the waveform tomography reconstruction using the TV or modified TV regularization schemes yields better approximated values to its true value of 1545 m/s and well preserves the edges of the tumors. However, the waveform tomography reconstruction result with the conventional TV regularization is much more oscillatory than the result obtained with ultrasound waveform tomography with the modified TV regularization. Therefore, the waveform tomography reconstruction with the modified TV regularization produces an even more accurate value of the sound speed than that using the conventional TV regularization.

[0216] In order to study the resolution of our new ultrasound waveform tomography method for tumors with small sizes, we created four numerical breast phantoms with different diameters ranging from 0.75 mm (about a half of a wavelength) to 4.5 mm (about 3 wavelengths). The tumors diameters in millimeters are 0.75 and 1.5; 1.5 and 2.25; 3.0 and 3.75; 3.75 and 4.5. The sound speeds of the background medium, small tumor and large tumor, are set to be 1500 m/s, 1540 m/s and 1560 m/s.

[0217] Besides the 2D reconstruction results, we also show the two horizontal profiles across the centers of the two tumors. As illustrated in FIG. **31**A through FIG. **31**C and FIG. **32**A through FIG. **32**D, we observe that the ultrasound waveform tomography method with the modified TV regularization can characterize tumors as small as about a half of an ultrasound wavelength. As we gradually increase the sizes of the tumors, as in FIG. **33**A through FIG. **33**C and FIG. **34**A through FIG. **34**D, FIG. **35**A through FIG. **35**C and FIG. **36**A through FIG. **36**D, and FIG. **37**A through FIG. **37**C and FIG. **38**A through FIG. **38**D, our method consistently provides accurate reconstructions of sound speeds and the shapes of the tumors.

[0218] In summary, the synthetic-aperture ultrasound tomography systems and methods of the present invention acquire ultrasound transmission and reflection data at the same time, and we have demonstrated that ultrasound waveform tomography using both ultrasound transmission and reflection data simultaneously greatly improves tomographic reconstructions of shapes and sound-speeds of tumors compared to tomographic reconstructions using only transmission data or only reflection data, particularly when used with the modified TV regularization method of the present invention.

[0219] From the discussion above it will be appreciated that the invention can be embodied in various ways, including the following:

[0220] 1. A synthetic aperture ultrasound tomography imaging method for imaging a tissue medium with one or more ultrasound transducer arrays comprising a plurality of transducers, the method comprising: exciting a first transducer with plurality of transducers to generate an ultrasound field within the tissue medium; acquiring a transmission signal and a reflection signal from a second transducer within the one or more ultrasound transducer arrays; and generating an ultrasound waveform tomography image reconstruction using both the acquired reflection and transmission signals.

[0221] 2. A method as recited in any of the preceding embodiments, wherein said step of generating an ultrasound waveform tomography image reconstruction is a function of computing an acoustic wave property of the reflection and transmission signals by calculating a minimum mean square difference between observed and synthetic waveforms relating to the reflection and transmission signals.

[0222] 3. A method as recited in any of the preceding embodiments, wherein said image reconstruction is a function of:

$$E(m) = \min_m \{\|d - f(m)\|_2^2\},$$

where $\|d-f(m)\|_2^2$ comprises a misfit function, and d comprises data relating to the acquired reflection signal and transmission signals.

[0223] 4. A method as recited in any of the preceding embodiments, further comprising performing total-variation regularization to generate sound-speed reconstructions of the acquired reflection and transmission signals.

[0224] 5. A method as recited in any of the preceding embodiments 4, wherein said total-variation regularization comprises a misfit function.

[0225] 6. A method as recited in any of the preceding embodiments, further comprising obtaining a gradient of the misfit function using an adjoint state method.

[0226] 7. A method as recited in any of the preceding embodiments, wherein said total-variation regularization is a function of:

$$E(m) = \min_m \{\|d - f(m)\|_2^2 + \lambda\|m\|_{TV}\},$$

and

where $\|d-f(m)\|_2^2$ comprises a misfit function, d comprises data relating to the acquired reflection signal and transmission signals, λ, is a positive regularization parameter, and $\|m\|_{TV}$ is a TV regularization term.

[0227] 8. A method as recited in any of the preceding embodiments, wherein λ, is selected as a function of:

$$\lambda = \frac{\|d - f(m)\|_2^2}{r \cdot \|m\|_{TV}},$$

where $\|d-f(m)\|_2^2$ is a fidelity term, $\|m\|_{TV}$ is a regularization term and a value of r is defined to be the ratio between the data fidelity term and the regularization term.

[0228] 9. A method as recited in any of the preceding embodiments, wherein said total-variation regularization comprises a modified total-variation regularization that is a function of:

$$E(m, u) = \min_{m,u} \{\|d - f(m)\|_2^2 + \lambda_1\|m - u\|_2^2 + \lambda_2\|\nabla u\|_1\},$$

and where $\|d-f(m)\|_2^2$ comprises a data misfit function, d comprises data relating to the acquired reflection signal and transmission signal, where $\|_1$ and λ_2 are both positive regularization parameters, and u is an auxiliary variable.

[0229] 10. A method as recited in any of the preceding embodiments, wherein λ_1 and λ_2 are selected as a function of:

$$\lambda_i = \frac{\text{data fidelity term}}{r_i \cdot \text{regularization term}}, \; i = 1,2,$$

where the values of r_i are defined to be the ratio between the data fidelity term and the regularization term.

[0230] 11. A method as recited in any of the preceding embodiments: wherein said total-variation regularization comprises a cost function; and wherein said cost function is decomposed with a modified TV regularization into two regularization problems.

[0231] 12. A method as recited in any of the preceding embodiments, wherein said regularization problems comprise a L_2-norm-based Tikhonov regularization problem and a L_1-norm-based TV regularization problem.

[0232] 13. A method as recited in any of the preceding embodiments, wherein the misfit function is minimized using an alternating minimization algorithm.

[0233] 14. A method as recited in any of the preceding embodiments, wherein a nonlinear conjugate gradient (NCG) approach is used to solve for the Tikhonov regularization problem.

[0234] 15. A method as recited in any of the preceding embodiments, wherein a split-Bregman method is used to solve the L_1-norm-based TV regularization problem.

[0235] 16. A method as recited in any of the preceding embodiments: wherein the plurality of transducers are configured such that a first set of two or more transducers are positioned at an opposing spaced-apart orientation from a second set of two or more transducers such that the first set of two or more transducers face the second set of two or more transducers; wherein the first and second sets of two or more transducers are positioned at spaced-apart locations so as to allow for the tissue medium to be positioned in between the first and second sets of two or more transducers; and wherein the method further comprises: exciting a first transducer with the first set of two or more transducers to generate an ultrasound field within the tissue medium; and receiving a transmission signal and a reflection signal from at least the second set of two or more transducers.

[0236] 17. A method as recited in any of the preceding embodiments, further comprising receiving a reflection signal from all transducers in the one or more arrays.

[0237] 18. A method as recited in any of the preceding embodiments, further comprising simultaneously receiving the reflection and transmission signals from the second set of two or more transducers.

[0238] 19. A synthetic aperture ultrasound tomography imaging system for imaging a tissue medium with one or more ultrasound transducer arrays comprising a plurality of transducers, the system comprising: a processor; and programming executable on said processor and configured for: exciting a first transducer with plurality of transducers to generate an ultrasound field within the tissue medium; receiving a transmission signal and a reflection signal from a second transducer within the one or more ultrasound transducer arrays; and generating an ultrasound waveform tomography image reconstruction using both the acquired reflection and transmission signals.

[0239] 20. A system as recited in any of the preceding embodiments, wherein said step of generating an ultrasound waveform tomography image reconstruction is a function of computing an acoustic wave property of the reflection and transmission signals by calculating a minimum mean square difference between observed and synthetic waveforms relating to the reflection and transmission signals.

[0240] 21. A system as recited in any of the preceding embodiments, wherein the image reconstruction is a function of:

$$E(m) = \min_m \{\|d - f(m)\|_2^2\},$$

where $\|d-f(m)\|_2^2$ comprises a misfit function, and d comprises data relating to the acquired reflection signal and transmission signal.

[0241] 22. A system as recited in any of the preceding embodiments, wherein total-variation regularization is performed to generate sound-speed reconstructions of the acquired reflection and transmission signals.

[0242] 23. A system as recited in any of the preceding embodiments, wherein said total-variation regularization comprises a misfit function.

[0243] 24. A system as recited in any of the preceding embodiments, wherein a gradient of the misfit function is obtained using an adjoint state system.

[0244] 25. A system as recited in any of the preceding embodiments, wherein said total-variation regularization is a function of:

$$E(m) = \min_m \{\|d - f(m)\|_2^2 + \lambda\|m\|_{TV}\},$$

and

where $\|d-f(m)\|_2^2$ comprises a misfit function, d comprises data relating to the acquired reflection signal and transmission signals, λ, is a positive regularization parameter, and $\|m\|_{TV}$ is a TV regularization term.

[0245] 26. A system as recited in any of the preceding embodiments 22, wherein λ is selected as a function of:

$$\lambda = \frac{\|d - f(m)\|_2^2}{r \cdot \|m\|_{TV}},$$

where $\|d-f(m)\|_2^2$ is a fidelity term, $\|m\|_{TV}$ is a regularization term and a value of r is defined to be the ratio between the data fidelity term and the regularization term.

[0246] 27. A system as recited in any of the preceding embodiments, wherein said total-variation regularization comprises a modified total-variation regularization that is a function of:

$$E(m, u) = \min_{m,u} \{\|d - f(m)\|_2^2 + \lambda_1\|m - u\|_2^2 + \lambda_2\|\nabla_u\|_1\},$$

and

where $\|d-f(m)\|_2^2$ comprises a data misfit function, d comprises data relating to the acquired reflection signal and transmission signal, where λ_1 and λ_2 are both positive regularization parameters, and u is an auxiliary variable.

[0247] 28. A system as recited in any of the preceding embodiments, wherein λ_1 and λ_2 are selected as a function of:

$$\lambda_i = \frac{\text{data fidelity term}}{r_i \cdot \text{regularization term}}, \; i = 1, 2,$$

where the values of r_i are defined to be the ratio between the data fidelity term and the regularization term.

[0248] 29. A system as recited in any of the preceding embodiments: wherein said total-variation regularization comprises a cost function; and wherein said cost function is decomposed with a modified TV regularization into two regularization problems.

[0249] 30. A system as recited in any of the preceding embodiments, wherein said regularization problems comprise a L_2-norm-based Tikhonov regularization problem and a L_1-norm-based TV regularization problem.

[0250] 31. A system as recited in any of the preceding embodiments, wherein the misfit function is minimized using an alternating minimization algorithm.

[0251] 32. A system as recited in any of the preceding embodiments, wherein a nonlinear conjugate gradient (NCG) approach is used to solve for the Tikhonov regularization problem.

[0252] 33. A system as recited in any of the preceding embodiments, wherein a split-Bregman system to is used to solve the L_1-norm-based TV regularization problem.

[0253] 34. A synthetic system as recited in any of the preceding embodiments: wherein the plurality of transducers are configured such that a first set of two or more transducers are positioned at an opposing spaced-apart orientation from a second set of two or more transducers such that the first set of two or more transducers face the second set of two or more transducers; wherein the first and second sets of two or more transducers are positioned at spaced-apart locations so as to allow for the tissue medium to be positioned in between the first and second sets of two or more transducers; and wherein the programming is further configured for: exciting a first transducer with the first set of two or more transducers to generate an ultrasound field within the tissue medium; and receiving a transmission signal and a reflection signal from at least the second set of two or more transducers.

[0254] 35. A system as recited in any of the preceding embodiments 34, further comprising receiving a reflection signal from all transducers in the one or more arrays.

[0255] 36. A system as recited in any of the preceding embodiments, wherein the programming is further configured for simultaneously receiving the reflection and transmission signals from the second set of two or more transducers.

[0256] 37. A synthetic aperture ultrasound tomography imaging system for imaging a tissue medium, the system comprising: one or more ultrasound transducer arrays; said one or more ultrasound transducer arrays comprising a plurality of transducers; a processor; and programming executable on said processor and configured for: exciting a first transducer with plurality of transducers to generate an ultrasound field within the tissue medium; receiving a transmission signal and a reflection signal from a second transducer within the one or more ultrasound transducer arrays; and generating an ultrasound waveform tomography image reconstruction using both the acquired reflection and transmission signals.

[0257] 38. A system as recited in any of the preceding embodiments 37: wherein the plurality of transducers are configured such that a first set of two or more transducers are positioned at an opposing spaced-apart orientation from a second set of two or more transducers such that the first set of two or more transducers face the second set of two or more transducers; and wherein the first and second sets of two or more transducers are positioned at spaced-apart locations so as to allow for the tissue medium to be positioned in between the first and second sets of two or more transducers.

[0258] Embodiments of the present invention may be described with reference to flowchart illustrations of methods

and systems according to embodiments of the invention, and/or algorithms, formulae, or other computational depictions, which may also be implemented as computer program products. In this regard, each block or step of a flowchart, and combinations of blocks (and/or steps) in a flowchart, algorithm, formula, or computational depiction can be implemented by various means, such as hardware, firmware, and/or software including one or more computer program instructions embodied in computer-readable program code logic.

[0259] As will be appreciated, any such computer program instructions may be loaded onto a computer, including without limitation a general purpose computer or special purpose computer, or other programmable processing apparatus to produce a machine, such that the computer program instructions which execute on the computer or other programmable processing apparatus create means for implementing the functions specified in the block(s) of the flowchart(s).

[0260] Accordingly, blocks of the flowcharts, algorithms, formulae, or computational depictions support combinations of means for performing the specified functions, combinations of steps for performing the specified functions, and computer program instructions, such as embodied in computer-readable program code logic means, for performing the specified functions. It will also be understood that each block of the flowchart illustrations, algorithms, formulae, or computational depictions and combinations thereof described herein, can be implemented by special purpose hardware-based computer systems which perform the specified functions or steps, or combinations of special purpose hardware and computer-readable program code logic means.

[0261] Furthermore, these computer program instructions, such as embodied in computer-readable program code logic, may also be stored in a computer-readable memory that can direct a computer or other programmable processing apparatus to function in a particular manner, such that the instructions stored in the computer-readable memory produce an article of manufacture including instruction means which implement the function specified in the block(s) of the flowchart(s). The computer program instructions may also be loaded onto a computer or other programmable processing apparatus to cause a series of operational steps to be performed on the computer or other programmable processing apparatus to produce a computer-implemented process such that the instructions which execute on the computer or other programmable processing apparatus provide steps for implementing the functions specified in the block(s) of the flowchart(s), algorithm(s), formula(e), or computational depiction(s).

[0262] Although the description herein contains many details, these should not be construed as limiting the scope of the disclosure but as merely providing illustrations of some of the presently preferred embodiments. Therefore, it will be appreciated that the scope of the disclosure fully encompasses other embodiments which may become obvious to those skilled in the art.

[0263] In the claims, reference to an element in the singular is not intended to mean "one and only one" unless explicitly so stated, but rather "one or more." All structural, chemical, and functional equivalents to the elements of the disclosed embodiments that are known to those of ordinary skill in the art are expressly incorporated herein by reference and are intended to be encompassed by the present claims. Furthermore, no element, component, or method step in the present disclosure is intended to be dedicated to the public regardless of whether the element, component, or method step is explicitly recited in the claims. No claim element herein is to be construed as a "means plus function" element unless the element is expressly recited using the phrase "means for". No claim element herein is to be construed as a "step plus function" element unless the element is expressly recited using the phrase "step for".

1. A synthetic aperture ultrasound tomography imaging method for imaging a tissue medium with one or more ultrasound transducer arrays comprising a plurality of transducers, the method comprising:

exciting a first transducer with plurality of transducers to generate an ultrasound field within the tissue medium;

acquiring a transmission signal and a reflection signal from a second transducer within the one or more ultrasound transducer arrays; and

generating an ultrasound waveform tomography image reconstruction using both the acquired reflection and transmission signals.

2. A method as recited in claim **1**, wherein said step of generating an ultrasound waveform tomography image reconstruction is a function of computing an acoustic wave property of the reflection and transmission signals by calculating a minimum mean square difference between observed and synthetic waveforms relating to the reflection and transmission signals.

3. A method as recited in claim **2**, wherein said image reconstruction is a function of:

$$E(m) = \min_m \{\|d - f(m)\|_2^2\},$$

where $\|d-f(m)\|_2^2$ comprises a misfit function, and d comprises data relating to the acquired reflection signal and transmission signals.

4. A method as recited in claim **1**, further comprising performing total-variation regularization to generate sound-speed reconstructions of the acquired reflection and transmission signals.

5. A method as recited in claim **4**, wherein said total-variation regularization comprises a misfit function.

6. A method as recited in claim **5**, further comprising obtaining a gradient of the misfit function using an adjoint state method.

7. A method as recited in claim **4**, wherein said total-variation regularization is a function of:

$$E(m) = \min_m \{\|d - f(m)\|_2^2 + \lambda\|m\|_{TV}\},$$

and

where $\|d-f(m)\|_2^2$ comprises a misfit function, d comprises data relating to the acquired reflection signal and transmission signals, λ is a positive regularization parameter, and $\|m\|_{TV}$ is a TV regularization term.

8. A method as recited in claim **4**, wherein λ is selected as a function of:

$$\lambda = \frac{\|d - f(m)\|_2^2}{r \cdot \|m\|_{TV}},$$

where $\|d-f(m)\|_2^2$ is a fidelity term, $\|m\|_{TV}$ is a regularization term and a value of r is defined to be the ratio between the data fidelity term and the regularization term.

9. A method as recited in claim **4**, wherein said total-variation regularization comprises a modified total-variation regularization that is a function of:

$$E(m, u) = \min_{m,u} \{\|d - f(m)\|_2^2 + \lambda_1\|m - u\|_2^2 + \lambda_2\|\nabla_u\|_1\},$$

and

where $\|d-f(m)\|_2^2$ comprises a data misfit function, d comprises data relating to the acquired reflection signal and transmission signal, where λ_1 and λ_2 are both positive regularization parameters, and u is an auxiliary variable.

10. A method as recited in claim **4**, wherein λ_1 and λ_2 are selected as a function of:

$$\lambda_i = \frac{\text{data fidelity term}}{r_i \cdot \text{regularization term}}, \; i = 1, 2,$$

where the values of r_i are defined to be the ratio between the data fidelity term and the regularization term.

11-18. (canceled)

19. A synthetic aperture ultrasound tomography imaging system for imaging a tissue medium with one or more ultrasound transducer arrays comprising a plurality of transducers, the system comprising:

a processor; and

programming executable on said processor and configured for:

exciting a first transducer with plurality of transducers to generate an ultrasound field within the tissue medium;

receiving a transmission signal and a reflection signal from a second transducer within the one or more ultrasound transducer arrays; and

generating an ultrasound waveform tomography image reconstruction using both the acquired reflection and transmission signals.

20. A system as recited in claim **19**, wherein said step of generating an ultrasound waveform tomography image reconstruction is a function of computing an acoustic wave property of the reflection and transmission signals by calculating a minimum mean square difference between observed and synthetic waveforms relating to the reflection and transmission signals.

21. A system as recited in claim **20**, wherein the image reconstruction is a function of:

$$E(m) = \min_m \{\|d - f(m)\|_2^2\},$$

where $\|d-f(m)\|_2^2$ comprises a misfit function, and d comprises data relating to the acquired reflection signal and transmission signal.

22. A system as recited in claim **19**, wherein total-variation regularization is performed to generate sound-speed reconstructions of the acquired reflection and transmission signals.

23. A system as recited in claim **22**, wherein said total-variation regularization comprises a misfit function.

24. A system as recited in claim **23**, wherein a gradient of the misfit function is obtained using an adjoint state system.

25. A system as recited in claim **22**, wherein said total-variation regularization is a function of:

$$E(m) = \min_m \{\|d - f(m)\|_2^2 + \lambda\|m\|_{TV}\},$$

and

where $\|d-f(m)\|_2^2$ comprises a misfit function, d comprises data relating to the acquired reflection signal and transmission signals, λ is a positive regularization parameter, and $\|m\|_{TV}$ is a TV regularization term.

26. A system as recited in claim **22**, wherein λ is selected as a function of:

$$\lambda = \frac{\|d - f(m)\|_2^2}{r \cdot \|m\|_{TV}},$$

where $\|d-f(m)\|_2^2$ is a fidelity term, $\|m\|_{TV}$ is a regularization term and a value of r is defined to be the ratio between the data fidelity term and the regularization term.

27. A system as recited in claim **22**, wherein said total-variation regularization comprises a modified total-variation regularization that is a function of:

$$E(m, u) = \min_{m,u} \{\|d - f(m)\|_2^2 + \lambda_1\|m - u\|_2^2 + \lambda_2\|\nabla_u\|_1\},$$

and

where $\|d-f(m)\|_2^2$ comprises a data misfit function, d comprises data relating to the acquired reflection signal and transmission signal, where λ_1 and λ_2 are both positive regularization parameters, and u is an auxiliary variable.

28. A system as recited in claim **22**, wherein λ_1 and λ_2 are selected as a function of:

$$\lambda_i = \frac{\text{data fidelity term}}{r_i \cdot \text{regularization term}}, \; i = 1, 2,$$

where the values of r_i are defined to be the ratio between the data fidelity term and the regularization term.

29-38. (canceled)

* * * * *

专利名称(译)	超声波形断层扫描与电视正规化		
公开(公告)号	US20140364735A1	公开(公告)日	2014-12-11
申请号	US14/339728	申请日	2014-07-24
[标]申请(专利权)人(译)	洛斯阿拉莫斯国家安全有限责任公司		
申请(专利权)人(译)	洛斯阿拉莫斯国家安全，有限责任公司		
[标]发明人	HUANG LIANJIE LIN YOUZUO		
发明人	HUANG, LIANJIE LIN, YOUZUO		
IPC分类号	A61B8/08 G06T5/00 A61B8/15		
CPC分类号	A61B8/0825 G06T5/001 A61B8/15 A61B8/5207 A61B5/0073 A61B5/7275 A61B8/085 A61B8/13 A61B8/14 A61B8/145 A61B8/406 A61B8/4477 A61B8/4488 A61B8/4494 A61B8/483 G01S15/8915 G01S15/8929 G01S15/8997 G06T11/005		
优先权	61/594865 2012-02-03 US		
外部链接	Espacenet USPTO		

摘要(译)

使用扫描阵列和算法的合成孔径超声断层摄影系统和方法被配置为同时获取超声传输和反射数据，并处理该数据以用于改进的超声断层摄影成像，其中断层摄影成像包括全变化正则化或修改的总变差正则化。